

ABSTRACT

Title of Document: OMI TROPOSPHERIC SULFUR DIOXIDE
RETRIEVAL: VALIDATION AND
ANALYSIS

Brittany Katherine McClure, Master of
Science, 2007

Directed By: Professor Russell Dickerson, Department of
Chemistry and Biochemistry, Department of
Atmospheric and Oceanic Science.

SO₂ impacts the radiative balance of the Earth and is the precursor to the major acid and much of the particulate matter in the atmosphere. Improved spectrometer resolution of the Ozone Monitoring Instrument (OMI) enables SO₂ retrieval in the planetary boundary layer. OMI has a small spatial resolution of 13 km x 24 km and daily near-global coverage. I have evaluated the accuracy of the OMI by comparing aircraft measurements in Northeast China to the OMI retrieval of three different algorithms: the Band Residual Difference (BRD), the Spectral Fit (SF), and a combination of the two (SF & BRD).

The SF algorithm shows the best agreement with a less than 15% difference for high SO₂ loading (greater than 1 DU). The SF & BRD has a ~ -0.25 DU bias, the BRD and SF a ~ -0.1 DU bias. The noise of the OMI is reduced to ~0.2 DU by averaging over 100 days and is not improved by increasing the averaging time. The OMI is also able to track SO₂ as it moves away from its source region in the PBL and once it is lofted above this layer.

OMI TROPOSPHERIC SULFUR DIOXIDE RETREIVAL: VALIDATION AND ANALYSIS

By

Brittany Katherine McClure

Thesis submitted to the Faculty of the Graduate School of the
University of Maryland, College Park, in partial fulfillment
of the requirements for the degree of
Master of Science
2007

Advisory Committee:
Professor Russell Dickerson, Chair
Dr. Jack Tossell
Dr. John Ondov
Dr. Nickolay Krotkov

© Copyright by
Brittany Katherine McClure
2007

ACKNOWLEDGEMENTS

I would like to thank...

my advisors, Russell Dickerson and Nickolay Krotkov, for all their time, advice, and allowing me to dive headfirst into research.

Jennifer Hains for her advice, her patience with my incessant questioning, and her wonderful idl programs and knowledge.

Can Li for his quick, accurate answers and ideas.

Simon Carn for setting up omiplot on my computer and converting files for me until I learned how to do it.

My teachers for all the new knowledge aquired in their classes.

NASA for funding my research.

Laura McClure, for reading through my countless papers tirelessly without complaint.

Joshua Overmiller for making me talk about my thesis so I could get everything straight in my head and for his support and encouragement.

And finally, the rest of my family for supporting me throughout.

Thank you!

TABLE OF CONTENTS

TABLE OF CONTENTS.....	iii
LIST OF TABLES.....	iv
LIST OF FIGURES.....	v
INTRODUCTION.....	1
CHAPTER 1: Airplane Analysis.....	9
1.1 Airplane Data Collection.....	9
1.2 Airplane Data Analysis.....	11
1.3 Airplane Error Analysis.....	13
CHAPTER 2: Ozone Monitoring Instrument (OMI).....	14
2.1 OMI Specifications and Air Mass Factor (AMF).....	14
2.2 Air Mass Factor.....	15
2.3 Band Residual Difference (BRD) Algorithm.....	16
2.4 Spectral Fit (SF) Algorithm.....	16
2.5 Spectral Fit and Band Residual Difference (SF & BRD) Algorithm.....	17
CHAPTER 3: OMI Error estimation.....	18
3.1 South Pacific.....	18
3.2 North Pacific.....	20
3.3 North America.....	21
3.4 Conclusions.....	23
CHAPTER 4: Validation Study.....	28
4.1 1 April 2005.....	28
4.2 5 April 2005.....	30
4.3 7 April 2005.....	32
4.4 10 April 2005.....	35
4.5 Comparisons and Discussion.....	35
CHAPTER 5: Trajectory Analysis.....	37
5.1 Air Mass Trajectory Determination.....	37
5.2 Plume Trajectory, 5-8 April 2005.....	38
5.3 SO ₂ mass calculations.....	40
5.3 Lifetime and Dispersion.....	41
5.4 Conclusions.....	43
CHAPTER 6: Discussion.....	44
CHAPTER 7: Future Work.....	46
WORKS CITED.....	48

LIST OF TABLES

Table 1.....	19
<i>Mean SO₂ values for 1-10 April 2005 over the South Pacific</i>	
Table 2.....	21
<i>Mean SO₂ values for 1-10 April 2005 over the North Pacific</i>	
Table 3.....	22
<i>Mean SO₂ values for 1-10 April 2005 over North America</i>	
Table 4.....	22
<i>Mean SO₂ values over three clean regions for 6 month and one year time periods</i>	
Table 4a.....	25
<i>Seasonal SO₂ mean and standard deviation values for three clean regions</i>	
Table 5.....	35
<i>SO₂ column contents determined from the airplane and the OMI retrieval algorithms (BRD, SF, SF&BRD)</i>	
Table 6.....	35
<i>Percent differences between airplane measurements and algorithm retrievals</i>	
Table 7.....	40
<i>SO₂ height from 5-8 April 2005 during plume trajectory analysis</i>	
Table 8.....	40
<i>SO₂ mass from 5-8 April 2005 during plume trajectory analysis with and without AMF corrections applied</i>	
Table 9.....	42
<i>Background box error estimation for SO₂ mass calculations using the BRD algorithm</i>	

LIST OF FIGURES

Figure 1a.....	4
<i>SO₂ spectrum at 273K between 285-325 nm.</i>	
Figure 1.....	10
<i>Map of Eastern China</i>	
Figure 2.....	11
<i>Airplane flight path on 5 April 2005</i>	
Figure 3.....	16
<i>AMF regression corrections for 5 April 2005 over Liaozhung</i>	
Figure 4.....	19
<i>Histogram of 1 Jan-30 June 2005 data over the South Pacific</i>	
Figure 5.....	20
<i>World map of 2005 average SO₂ column contents from the OMI</i>	
Figure 6.....	21
<i>Histogram of 1 Jan-30 June 2005 data over the North Pacific</i>	
Figure 7.....	22
<i>Histogram of 1 Jan-30 June 2005 data over North America</i>	
Figure 8.....	23
<i>Standard deviation and reflectivity versus Julian day over N. America, N. Pacific, and S. Pacific regions in 2005..</i>	
Figure 9.....	24
<i>Sigma prime versus number of days over all three clean regions in 2005</i>	
Figure 10.....	29
<i>Airplane and the OMI retrievals for the BRD, SF, and BRD&SF algorithms on 1 April 2005 over 41 43°N, 122 124°E (sampling region)</i>	
Figure 11.....	30
<i>24-hour Hysplit back trajectories on 1 and 5 April 2005 from the airplane sampling region</i>	
Figure 12.....	31
<i>Airplane and the OMI retrievals for the BRD, SF, and BRD&SF algorithms on 5 April 2005 over 41 43°N, 122 124°E</i>	
Figure 13.....	32
<i>24-hour Hysplit back trajectories on 7 and 10 April 2005 from the airplane sampling region</i>	
Figure 14.....	33
<i>Airplane and the OMI retrievals for the BRD, SF, and BRD&SF algorithms on 7 April 2005 over 41 43°N, 122 124°E</i>	
Figure 15.....	34
<i>Airplane and the OMI retrievals for the BRD, SF, and BRD&SF algorithms on 10 April 2005 over 41 43°N, 122 124°E</i>	
Figure 16.....	39
<i>72-hour forward Hysplit trajectory from airplane sampling region, AMF regression for lofted SO₂, and corrected SO₂ pictures on 6 April 2005</i>	
Figure 17.....	41
<i>OMI retrievals using the BRD algorithm from 5-8 April 2005 monitoring plume motion</i>	

Figure 18.....	43
<i>SO₂ lifetime plot</i>	
Figure 19.....	47
<i>Collection 2 versus Collection 3 data retrieval on 1 April 2005</i>	

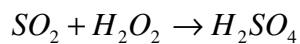
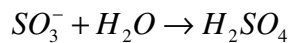
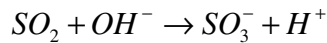
INTRODUCTION

As the sophistication of science and technology increases, so does the desire for an improved understanding of the world around us. In predicting the future of our planet, all aspects of the globe are being examined from the oceans to the atmosphere. Changes made by human activity on land are believed to have an impact on the atmosphere over both the land and sea. Human activity has led to an increase in fossil fuel burning (coal, oil, and natural gas), ore smelters (mainly copper) and other industrial processes (Cullis, 1980, Streets et al., 2000). These actions produce large amounts of radiative forcing atmospheric gases such as SO₂ and release them into the atmosphere. In China most of the SO₂ emissions are concentrated along the Eastern coast (Guttikunda et al., 2005, Heald et al., 2003) and have been steadily increasing (Streets et al., 2000, Luo et al., 2000).

SO₂ released as a result of human activity is usually emitted below 3 km in a region called the planetary boundary layer (PBL). The PBL may be defined as the layer below the height of a temperature inversion in the atmosphere. This height rises during the day as the ground heats up and lowers at night forcing many gases and aerosols to settle out of the atmosphere by dry deposition. Therefore, in order for SO₂ to have a large atmospheric impact it must be transported out of the PBL during the day by convection or the Warm Conveyor Belt Circulation (WCB). WCB is when air moves up along lines of constant entropy ahead of a cold front (as described in Dickerson et al., 2007). Once lofted above the PBL into the free troposphere (FT), SO₂ has been shown to have a lifetime of 0.6-2.6 days before turning into sulfate or settling out of the atmosphere. (Pham et al., 1995, Chin et al., 1996, Koch et al., 1999, Roelofs et al., 1998, Berglen et

al., 2004, Hains et al., 2007). This can have a large impact on the radiative forcing (cooling or warming effect) of the Earth's surface.

There are many pathways through which this may be done. Currently identified pathways lead to the formation of sulfate aerosols from the SO₂ molecule. These pathways include:



(Finlayson and Pitts, 1976). The reactions with hydroxide and water occur in clouds in the aqueous phase. SO₂ reacts with OH⁻ in the gaseous phase and may also react with ozone in cloud water in the free troposphere (Benkovitz et al, 2006).

Once a sulfate molecule is formed, it can serve as cloud condensation nucleus. The difference between water vapor droplets nucleating on sulfate aerosols versus on ice crystals is that the droplets formed on sulfate are much smaller. This means there is less precipitation even though more clouds form (Qian et al., 2006). This decrease in precipitation not only changes the water balance in the region but also allows the clouds to remain as a solar barrier between the Earth and the sun, decreasing the radiation that reaches the surface. This creates a net-cooling force on the Earth.

When it does rain, the water droplets react to form sulfuric acid, creating acid rain, which has a low pH. Acid rain has environmental impacts on plants, soil, water pathways, and human health because it hinders plants' growth abilities, depletes soil of its nutrients, contaminates the water, and increases paint and cement degradation rates (Gondal, 2001, EPA, 2007, Xu et al, 2007). Prolonged high SO₂ concentrations are

believed to have a direct impact on human health as a result of particle inhalation, which is thought cause birth defects (Gilboa, 2005).

Measuring SO₂ on a global scale is an important piece of the global climate puzzle due to its cooling effects and environmental impacts. Previous satellite measurements have not been accurate enough to measure SO₂ concentrations in the troposphere. The spatial resolution of most satellites is not small enough to determine trace gas quantities at such a large distance from the measurement source. NASA's heritage instrument Total Ozone Mapping Spectrometer (TOMS) had a spatial resolution of 50 km x 50 km in nadir. The European UV spectrometers, Global Ozone Monitoring Experiment (GOME) and Scanning Imaging Absorption Spectrometer for Atmospheric Chartography (SCIAMCY), have spatial resolutions of 40 km x 320 km and 30 km x 400 km nadir respectively. These large footprints don't allow the instruments to see between clouds, making measurements in the PBL very difficult. Also, both GOME and SCIAMCY take several days to acquire a continuous global map (Eisinger 1998; Bovensmann et al. 1999; Burrows et al 1999). Due to the limitations of these satellites, anthropogenically produced SO₂ is not well studied and its long-term effects are still being determined. Increased knowledge of SO₂ global emissions and transport are necessary for an improved global understanding of the atmosphere. The Ozone Monitoring Instrument (OMI) launched aboard AURA in July 2004 has a smaller spatial resolution (13 km x 24 km in nadir) than previous satellites. It also has daily global coverage.

SO₂ is measured by satellites using Differential Optical Absorption Spectroscopy. DOAS was introduced in 1975 and 1979 by Noxen and Platt (Noxon et al., 1978, Noxon, 1975, Platt 1979, Platt et al., 1980). DOAS measures the change in radiation between the

output and the input signal. When radiation hits SO₂ the energy is absorbed by the

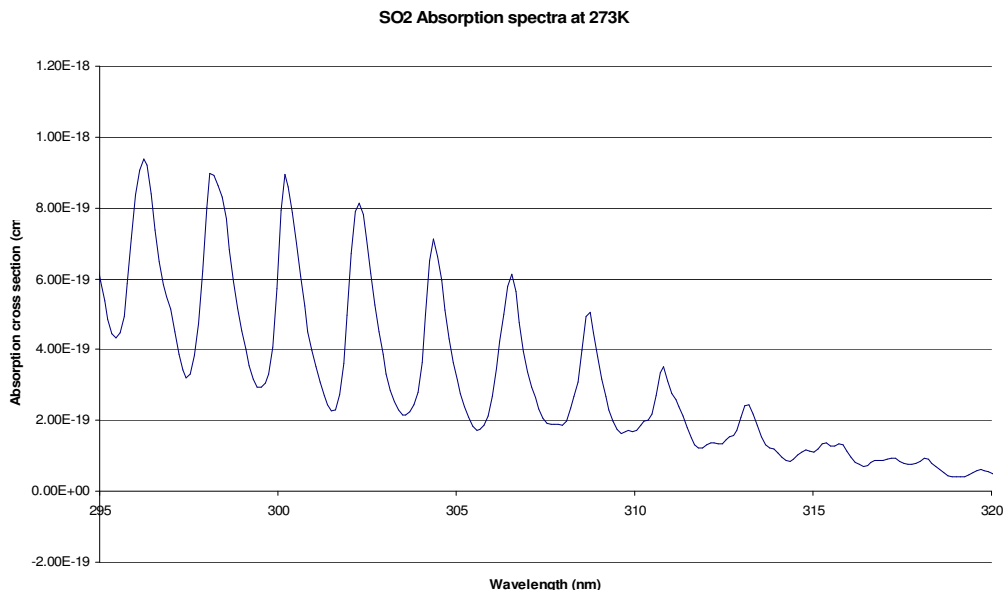


Figure 1a: SO₂ absorption spectrum at 273 K (Bogumil et al., 2003).

molecule, moving it to an excited state. A sample SO₂ spectrum is shown in Figure 1a. The transitions seen in Figure 1a correspond to the ¹A₁ symmetry group of SO₂ (a C_{2v} molecule) changing into ¹B₁ and ¹A₂ symmetry groups due to photon absorption. DOAS uses a continuous light source to send a signal into the atmosphere. The light is then received back from the atmosphere. The light source can be the sun or a lamp such as a Xe-arc lamp. Satellites use the sun as a light source. The detector can be set up at long distances from the desired detection region (i.e. from space). A very long path length can cause many difficulties in determining the true signal. This will be discussed in more detail later in this section. Sunlight is scattered and absorbed by molecules in the air depending on their size and distance. A slotted disk rotates before the input, to scan the spectrum over some integration time (i.e., 0.04 s), allowing nearly simultaneous

measurement of many species in the spectral range. The slant column density, S , of a DOAS measurement is defined as

$$S = \int_0^L c(l)dl \quad (1)$$

where L is the path length of the light and $c(l)$ is the concentration of species along the path. The light is then collected by a detector. One type of detector, a charge-coupled device (CCD), is first used by the OMI because of its ability to measure many species simultaneously without the need for a scan mirror. A CCD is a two dimension array made from silicion which contains light-sensitive picture elements (pixels). The electronic charges created by light absorption are stored in each pixel.

SO₂ detection on the GOME, SCHIAMCY use DOAS (Platt et al., 1999) and the OMI aboard AURA uses a UV/VIS nadir solar backscatter spectrometer (which is similar to DOAS). Trace gas detection from space is much more complicated due to the long path length, quantity of interfering particles, the viewing geometry, and cloud cover. On the OMI, solar irradiance is I_0 measured directly at varying angles through a diffuser. There are three different diffusers on the OMI: one quartz volume and two aluminum diffusers. When the solar aperture mechanism is opened once a day, the light from the sun passes through a mesh to reduce the solar irradiance by a factor of 10 so that the detectors will not become saturated, enabling the input to be determined. The aluminum diffusers are used for weekly and monthly measurements while the quartz volume diffuser is used daily. After the irradiance passes through the diffuser it is reflected off a folding mirror to the detector allowing the initial signal (the solar irradiance) to be

determined. When solar radiation passes through the solar photosphere it is absorbed creating Fraunhofer lines (FRL).

FRL measured in nadir are used for spectral calibration. These lines are believed to be caused by Rotational Raman scattering. The strength of the lines depends on the solar zenith angle (sza) which is called the Ring Effect. The ring effect describes that the strength of the FRL lines decrease as the sza increases from nadir. Therefore, Ring spectrum must be included in fitting calculations (Stutz and Platts, 1996).

When the Earth's radiance is collected by the OMI, the light passes through a scrambler essentially depolarizes the signal (though it is not a truly depolarized signal) and making it insensitive to the instrument polarization sensitivity that GOME and SCHIAMACY had. Once the signal is split by a dichronic mirror into UV-1, UV-2, and VIS channels, it is measured by a 2-D silicon CCD encased in aluminum to keep stray particles away from the CCD. One dimension of the array collects the spectral information (780 pixels) and the other dimension collects the spatial information (576 pixels), thereby allowing the instrument to function without the scan mirror needed in GOME and SCHIAMACY. The instrument is calibrated once a day using green-light emitting diodes to determine the bad CCD pixels, the electronic gain, and the non-linearity effects. A WLS (tungsten halogen lamp with quartz bulb) is used to determine the pixel-to-pixel variations, the detector non-linearity, and the radiometric degradation. The optical bench (which houses the CCD) is kept at 265 K via heaters. The signal from the CCD is then sent via a video signal to the electronics unit (ELU) to turn it into a digital signal (Levelt et al. 2006, Dobber et al. 2006). Once the signal is converted to radiance data, algorithms may be applied to it. SO₂ is first retrieved as slant column

values (SCD) and therefore must be divided by an air mass factor (AMF) to determine the vertical column values (VCD).

The AMF is defined as

$$AMF = \frac{SCD}{VCD} \quad (2)$$

where VCD is the vertical column density. The AMF depends on gas concentration, vertical profile distribution, surface reflectivity (albedo), aerosol loading, and viewing geometry. Honninger et al. (2004) demonstrated the AMF dependence on sample and aerosol height, loading, type, and distribution. Clouds also hinder SO₂ measurements as the reflectivity is too high to have an accurate measure of the actual signal below the clouds. However, clouds can increase OMI sensitivity if SO₂ is above them. In the OMI SO₂ PBL product (OMSO2) (publicly available), pixels with more than a 30% reflectivity are not used in mass calculations but rather fill values are used for these pixels (Krotkov et al., 2006, Krotkov et al., 2007)

This paper will discuss three different algorithms for SO₂ retrieval from the OMI. The first is the operational PBL OMSO2 product which uses a Band Residual Difference algorithm based on the algorithm developed for Total Ozone Mapping Spectrometer (TOMS) (Krotkov et al., 2006, Bhartia et al., 2002). This algorithm is especially sensitive to absolute radiance measurements. The second algorithm is the Spectral Fit algorithm that is currently applied off-line and is under evaluation. Thirdly, a combination of these two algorithms is discussed. To determine the noise of the algorithms, three regions with zero SO₂ loading are analyzed over varying time periods. The accuracy is investigated by comparing *in situ* aircraft measurements with the results

from the algorithms. In early April 2005, SO₂ was measured during the East Asian Study of Troposphere Aerosols- An International Regional Experiment (EAST-AIRE) campaign between 0-4 km over Eastern China in the Shenyang region (Figure 1). These retrievals over China are of particular importance due to the high SO₂ loading. The BRD algorithm is used to track an SO₂ plume for 3 days as it traveled away from China out to the Pacific Ocean to determine the lifetime of SO₂ and the ability of the OMI to track plume movement.

CHAPTER 1: Airplane Analysis

1.1 Airplane Data Collection

During the EAST-AIRE campaign in early April 2005, aircraft flights measured trace gases and aerosol concentrations over North Eastern China. These flights were made on a Chinese Y-12 twin engine turboprop plane. Two inlets were located on top of the cockpit in front of the engines; a forward facing isokinetic inlet to collect aerosols and a backward facing inlet for trace gas measurements. SO₂ was measured using a modified commercial (Luke 1997) pulse-fluorescence detector (Thermo Environmental Instruments Model 43 C). Relative humidity and temperature were measured with a probe (EIL Instruments Inc., Rustrak RR2-252, Hunt Valley, MD) and pressure with a Rosemount Model 2005 Pressure Transducer. Location was monitored with a Global Positioning System receiver (Garmin GPS-90). Other instruments on board have been previously described in more detail (Taubman 2004; Dickerson et al. 2006).

Eight flights were completed between 1 April 2005 and 12 April 2005 in the region shown in a green box in Figure 1. The flight paths and more detailed flight information can be found at www.atmos.umd.edu/~yuan/web_proj/air_camp/air_camp.htm. All flights departed from

Taoxian International Airport (41.640°N, 123.488°E) in the Shenyang region of China.



Figure 1: Map of Eastern China. The box in green around Shenyang and Fushun shows the region of the flight path as shown more detail in Figure 2 (Encyclopedia Britannica 2002).

Four of these flights performed spirals to determine column contents in the lower troposphere. On 5 April 2005 the aircraft departed at 18:10 UTC and headed south, away from the Shenyang region. Two ascending spirals were performed during the flight over farmland, from about 300m up to about 4000m above sea level at 42.450°N, 123.70°E (Xiaoming) and 41.350°N, 122.648°E (Liaozhung). The flight path is shown in Figure 2.

Flight paths on 7 and 10 April 2005 were similar to that of 5 April, with spirals in the same locations. Column contents can also be determined from the landing pattern of the airplane on these days. On 1 April 2005, the airplane did not perform spirals in the same locations but did descend into the airport at a rate that may be used for column content analysis.

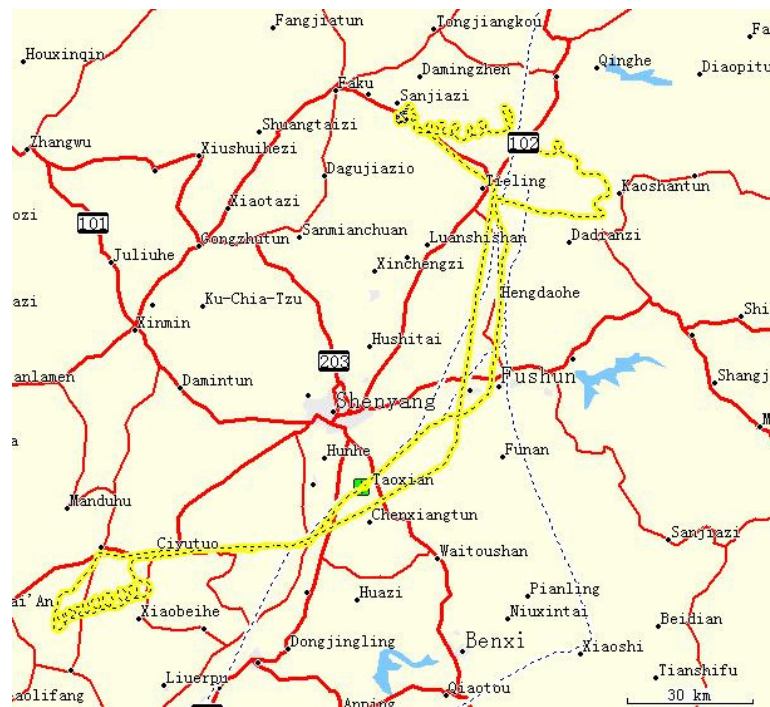


Figure 2: An inset of the green box in Figure 1 showing the flight path on 5 April 2005.

1.2 Airplane Data Analysis

The voltages read by the SO₂ detector were converted to SO₂ mixing ratios in ppb using a calibration factor. A 5.5 ppmv SO₂ in air (Scott-Martin, Riverside, CA) calibration gas was diluted to mixing ratios of 0.0, 1.6, 11.0, 20.8, 35.6, 55.2, 74.8, and

99.0 ppb on 20 May 2005. These known ratios were measured by the SO₂ detector. The calibration factor determined from the known mixing ratios and SO₂ detector reading was 4.19. The data was converted from volts to ppb using a calibration factor of 4.1 (personal communication with Can Li). The R² value of this curve is 0.99, nearly 1.0, making the error associated with this calculation negligible.

Mixing Ratios (ppb) determined from the calibration were then turned into column content values using the formula

$$Partial\ Pressure(atmm) = \int_{z_1}^{z_2} ppbSO_2 \times 10^{-9} \times \frac{Palt(mbar)}{1013.25(mbar/atm)} \times \frac{273}{T(^{\circ}C) + 273} dz$$

where z_1 and z_2 denote the minimum and maximum column altitudes in meters (m). The purpose of this conversion is to determine the column content of SO₂ in Dobson Units (DU). A Dobson Unit is defined as 2.69×10^{16} molecules/cm². In calculating the column content, 100 m intervals were used for each layer and then these values were added together to determine the total column content of SO₂ in the region in question. For example, $z_1 = 100$ m and $z_2 = 200$ m, and the partial pressure (atm-m) is calculated for a region. This is repeated until the top of the sampling region and these values are added to determine the total column amount. Missing values of pressure and temperature were assumed to be the average values of temperature and pressure found during the EAST-AIRE campaign in each 100 m height interval.

1.3 Airplane Error Analysis

SO₂ was measured using a modified commercial (Luke 1997) pulse-fluorescence detector (Thermo Environmental Instruments Model 43 C). The minimum detection limit of the SO₂ monitor is 0.08 ppb. The data were corrected so that all the measurements below the minimum detection limit were set to half of this limit. Doing this removed negative values and steadied the noise of the system. Luke et al (1997) determined the uncertainty of the aircraft values to be 16% with a 95% confidence level for SO₂ measurements between 0.18 and 0.5 ppb. The uncertainty becomes smaller for larger SO₂ mixing ratios. The contributions for this uncertainty include sampling line loss, instrument noise, and interference by other species.

CHAPTER 2: Ozone Monitoring Instrument (OMI)

2.1 OMI Specifications and Air Mass Factor (AMF)

The Ozone Monitoring Instrument (OMI) completes 14 orbits a day at a 98.2° inclination and with a sun-synchronized polar orbit. The DOAS spectrometer measures in the UV/VIS splitting the UV into two channels to reduce the stray light in the higher frequencies (below 290 nm). The UV-2 channel has a performance range of 310-365 nm allowing it to measure SO₂ (310-315 nm). The OMI field of view is 114° which leads to a 2600 km swath width perpendicular to the flight direction. In the normal global mode, 5 measurements of 0.4 sec are co-added for a total exposure time of 2 seconds. This results in 13 km in the direction of flight. Together, the total ground pixel size of the OMI is 13 km x 24 km at nadir and ranges up to 25 km x 150 km though the pixel size remains relatively constant and increases sharply at larger distances from nadir. This small pixel size allows OMI to see the troposphere better than its predecessors (Levelt et al., 2006). When discussing SO₂ retrieval using the various algorithms, the SO₂ is considered to be in the PBL unless otherwise noted. The publicly released OMI SO₂ data (version 1) uses a Band Residual Difference (BRD) algorithm (Krotkov et al, 2006). Two other offline algorithms are also evaluated: a Spectral Fit (SF) algorithm developed by Kai Yang and a combination of SF and BRD algorithms.

2.2 Air Mass Factor

These algorithms all utilize an air mass factor (AMF) to correct for geometric, ozone, aerosol, albedo, cloud, and SO₂ variation in a column. The AMF is a function of the observation geometry (view θ , solar zenith, θ_0 and azimuth ϕ angles), the SO₂ column amount, the surface albedo, R_s , total column ozone amount, Ω , cloud variations, and aerosols.

$$AMF = \int_0^{\infty} m(z', \Omega, \theta, \theta_0, \phi) \tilde{n}_{SO_2}(z') dz' \quad (3)$$

The $n(z')$ in equation 3 is the normalized vertical SO₂ profile. In all the algorithms, AMF is constant at 0.36. This value reflects ideal conditions with no cloud cover or aerosol loading, 5% surface reflectivity, slant column ozone of ~1000 DU, a 1 DU SO₂ loading with a typical vertical profile over the mid-Atlantic US region (Taubman et al, 2006), and 1 atm surface pressure. Offline AMF corrections have been used to try and improve the OMSO₂ product (Figure 3). In these corrections

$$SO_2(\text{corrected}) = \frac{0.36}{AMF(\text{regression})} \times SO_2(\text{operational}) \quad (4)$$

the AMF (regression) is determined using a linear parameterization of equation 2 based on the vertical SO₂ profile, the surface albedo, and the aerosol and/or cloud presence. The regression uses SCO measured by OMI rather than calculating $m(z)$ each time which would be time- and labor-intensive. When the SCO is greater than 1500 DU fill values must be used as the resulting AMF is too small for significant PBL SO₂ retrieval.

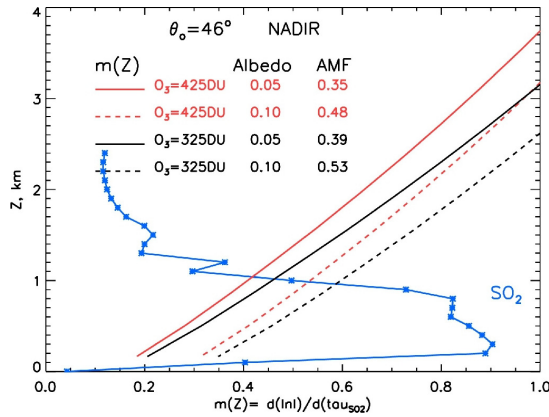


Figure 3: The AMF regressions for 5 April 2005 over Liaozhung as a function of altitude. The regressions assume a cloud-free and aerosol-free atmosphere at 312 nm. The solar zenith angle is 46° and the observation direction nadir. The red lines represent total column ozone of 425 DU, with the dashed line showing a 0.1 surface albedo and the solid line showing a 0.05 surface albedo. The black lines represent a 325 DU ozone column with 0.1 albedo dashed line and 0.05 surface albedo solid line. The blue curve is the normalized vertical SO_2 profile from 0-3km as determined by aircraft measurement (Krotkov et al, 2007).

2.3 Band Residual Difference (BRD) Algorithm

The BRD algorithm utilizes absorption band centers from the NASA operational ozone algorithm (OMTO3, Collection 2 OMI Level 1b data). At a constant temperature (275K), 3 pairs of residuals are converted to SO_2 slant column density using differential SO_2 cross section data (Bogumil et al 2000). Only values with a reflectivity of less than 30% are used. These slant column densities are converted to total vertical column amount by dividing them by an air mass factor (AMF). The column density is expressed in Dobson Units (DU) (Krotkov et al., 2006).

2.4 Spectral Fit (SF) Algorithm

The offline SF algorithm is a new development by the OMI SO_2 team. All the spectral measurements between 310.8 nm and 315.8 nm are used rather than just the three

pairs as is done in the BRD algorithm. The effects from atmospheric contributions such as reflectivity, ring effect, and ozone are removed, making the residuals proportional to the absorption cross section of SO₂. The output of the algorithm is the magnitude of these cross sections which yields the slant column SO₂ in DU (personal communication Kai Yang, 2007).

2.5 Combined Spectral Fit and Band Residual Difference (SF & BRD)

Algorithm

This analysis combines the two methods listed above. The wavelengths of the Spectral Fit are analyzed to determine the SO₂ residuals. Three pairs of these residuals are then used in the BRD algorithm to calculate the amount of SO₂ in the slant column. Though the algorithm runs the same as it does with the operational data, the input residuals are different, so it yields unique SO₂ column amounts.

CHAPTER 3: OMI Error estimation

The noise of the OMI is analyzed in this chapter by looking at three clean regions. These regions were determined by analyzing one- and two-year average SO₂ plots for assumed zero concentration regions with view angles of ~40°. The standard deviations given in the tables are the standard deviations of the area mean average SO₂ column content values.

3.1 South Pacific

SO₂ was measured in the box 40°S to 44°S, 128°E to 134°E. This box lies south of Australia in the South Pacific Ocean (red box, Figure 5) at about the same sza as the testing region in China. The region does not receive regular emissions from Australia or any other known SO₂ pollution sources. This was confirmed using a yearly SO₂ retrieval map (Figure 5) and Hysplit air mass trajectories. From 1 January 2005 to 30 July 2005 the average SO₂ in this region, using the BRD algorithm, was -0.1 ± 0.7 DU (see Table 4 for more details). This was calculated by determining one mean SO₂ value per box per day. These means were then averaged to determine the six month average. A histogram of the distribution of this data is shown in Figure 2. The data has a sharper peak than a Gaussian curve. This means the noise is not normally distributed around 0 but rather is skewed toward the mean value. This sort of distribution can be analyzed using its Kurtosis value. The Kurtosis shows the level of peakedness of the distribution of several measurements. A negative Kurtosis means the distribution is flatter than a Gaussian distribution and a positive kurtosis means the data is more peaked than a Gaussian

distribution. A Gaussian distribution has a zero Kurtosis. The magnitude of these numbers tells the extremity of the situation. In this instance, the Kurtosis is 1.6, highlighting the peakedness of the histogram.

SO₂ was also measured in the same box over a shorter time period (1-10 April, 2005) using all three algorithms. The results of the different algorithms are shown in Table 1.

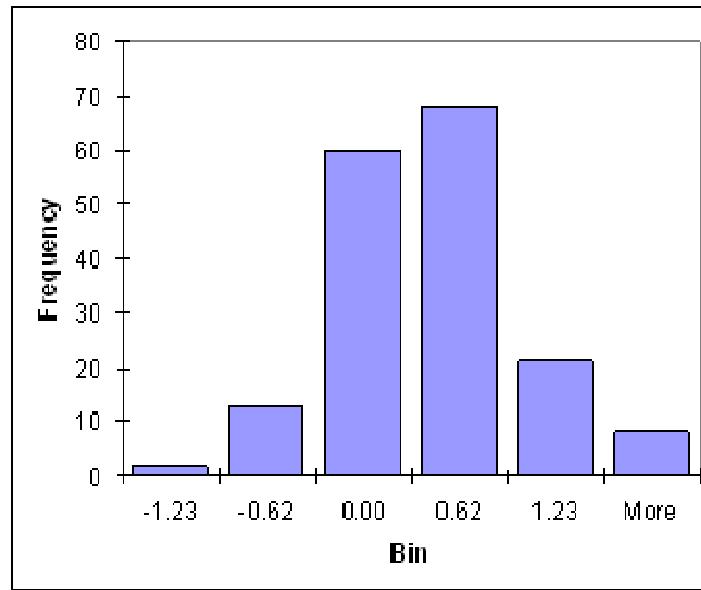


Figure 4: Distribution of the average SO₂ column loading over South Pacific [40°S 44° S, 128°E 134° E] from 1 Jan 2005 to 31 June 2005. The mean of these values is -0.1 ± 0.8 DU.

	Number Days	Mean (DU)	Standard Deviation (DU)	Kurtosis (column)
BRD	10	0.1	1.0	-0.5
SF	9	-0.1	0.6	0.9
SF & BRD	9	-0.2	0.6	1.6

Table 1: The mean values of SO₂ mass and column loading using the band residual difference (BRD) algorithm, the Spectral Fit algorithm (SF) and the combined SF and BRD algorithm over the South Pacific. Each mean value is for 1-10 April 2005. The SF and SF&BRD both exclude 9 April 2005 due to their being no Spectral Fit data for this day. The box for these values was 41°S 43° S, and 122°E 124° E.

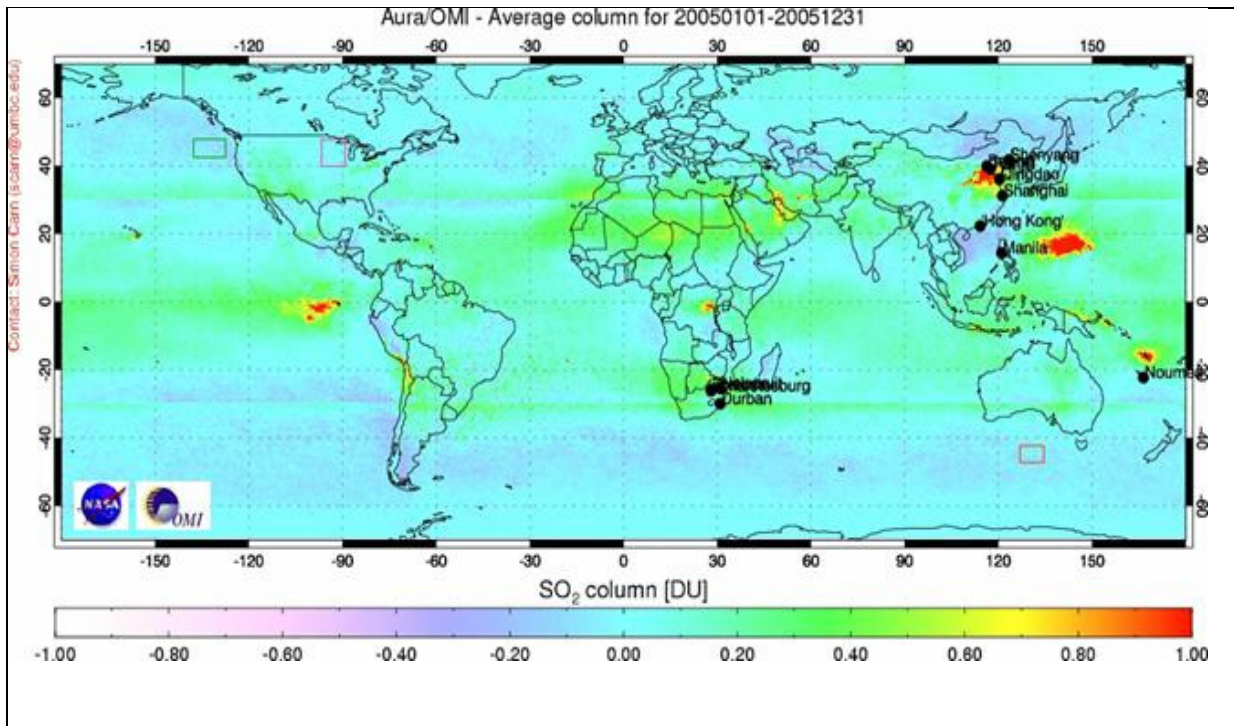


Figure 5: One year average column content of SO_2 for the world in 2005. The background regions are shown in boxes: the South Pacific region by a red box, the North Pacific region by a green box, and the North America region by a pink box.

3.2 North Pacific

The second region chosen for a background SO_2 analysis was in the North Pacific off the coast of California. This region should not have large amounts of SO_2 as it is far enough from California to not receive regular emissions from the state and should be far enough from Asia to not receive emissions from that region either. The box tested over the North Pacific was 41°N to 43°N and 130°W to 140°W . The mean over this region using the BRD algorithm from 1 January 2005 to 30 June 2005 was -0.2 ± 0.7 DU and over a year the mean got closer to 0, -0.1 ± 0.6 DU. The Kurtosis of both data sets is 1.5 (Figure 6). The distribution is non-Gaussian and closer to a logistic distribution (Kurtosis 1.2). This region was also analyzed from 1-10 April 2005 using all three algorithms. These results are shown in Table 2.

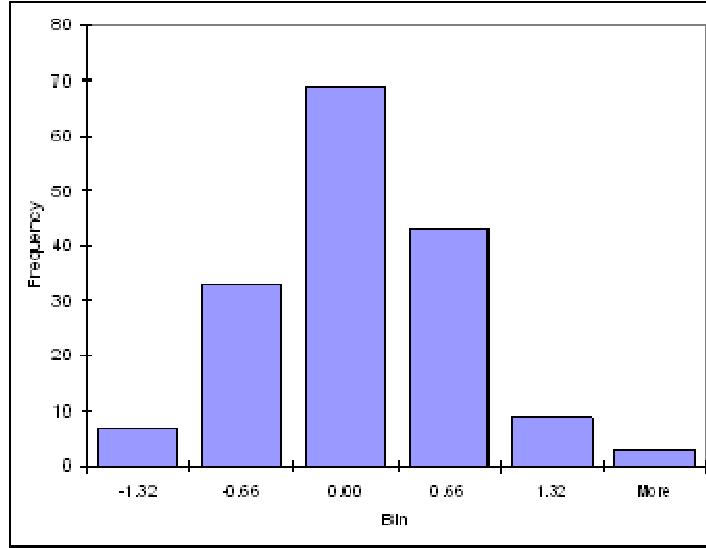


Figure 6: The distribution around 0 from the OMI using the BRD algorithm over the North Pacific [41 43°N, 130 140° W] for 1 Jan 2005 to 31 June 2005. The mean value is -0.2 ± 0.7 DU.

	<i>Number Days</i>	<i>Mean (DU)</i>	<i>Standard Deviation (DU)</i>	<i>Kurtosis (column)</i>
<i>BRD</i>	10	-0.07	0.6	1.5
<i>SF</i>	10	0.02	0.5	3.2
<i>SF & BRD</i>	10	-0.2	0.6	0.9

Table 2: The distribution of data for 1-10 April 2005 over the North Pacific using all three algorithms.

3.3 North America

The third clean region is over land in North America (40 50°N, 90 100°W). In both the one- and two-year averages, this region has a distribution around zero. Looking at the mean of 1 Jan 2005 to 31 June 2005, a negative value is seen, -0.3 ± 0.7 DU. Unlike the two oceanic regions, this distribution is close to Gaussian with a slightly

positive Kurtosis value of 0.8 (Table 4). 1-10 April 2005 averages for this region are shown in Table 3.

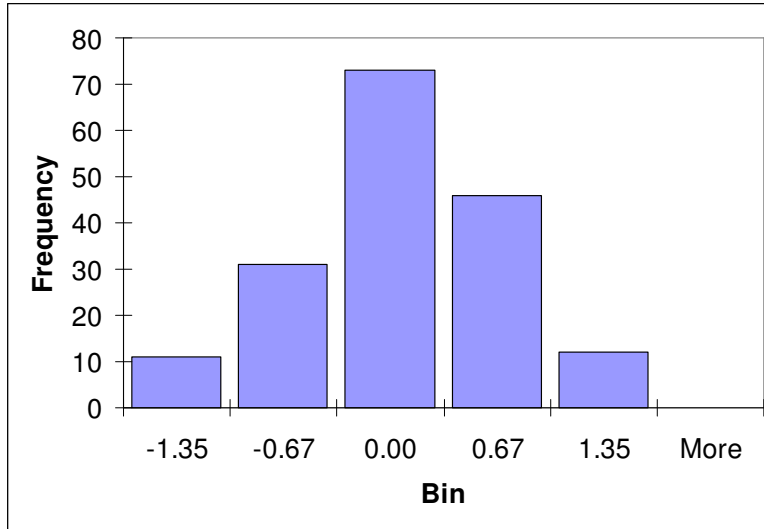


Figure 7: Average SO₂ distribution over North America [40 50°N, 90 100°W] for 1 Jan 2005 to 31 June 2005. The mean value is -0.30 ± 0.7 DU.

	<i>Number Days</i>	<i>Mean (DU)</i>	<i>Standard Deviation (DU)</i>	<i>Kurtosis (column)</i>
<i>BRD</i>	10	0.5	0.4	-0.3
<i>SF</i>	10	-0.06	0.3	2.1
<i>SF & BRD</i>	10	-0.3	0.4	1.7

Table 3: The distribution of data for 1-10 April 2005 over the North America using all three algorithms.

3.4 Comparisons

Location	Date	Count	Mean	Standard Deviation	Kurtosis
N. Pacific	1 Jan-30 June 2005	164	-0.2	0.7	0.8
N. Pacific	1 Jan-30 Dec 2005	338	-0.1	0.6	1.5
S. Pacific	1 Jan-30 June 2005	172	0.1	0.6	1.6
S. Pacific	1 Jan-30 Dec 2005	347	-0.1	0.7	1.1
N. America	1 Jan-30 June 2005	173	-0.3	0.7	0.8
N. America	1 Jan-30 Dec 2005	349	-0.1	0.6	1.8

Table 4: The statistics for the three background regions for 6- month and one-year time periods using the BRD algorithm. The latitude and longitudes for the regions are as follows: N. Pacific [41 43°N, 130 140°W], S. Pacific [40 44°S, 128 134°E], and N. America [40 50°N, 90 100°W].

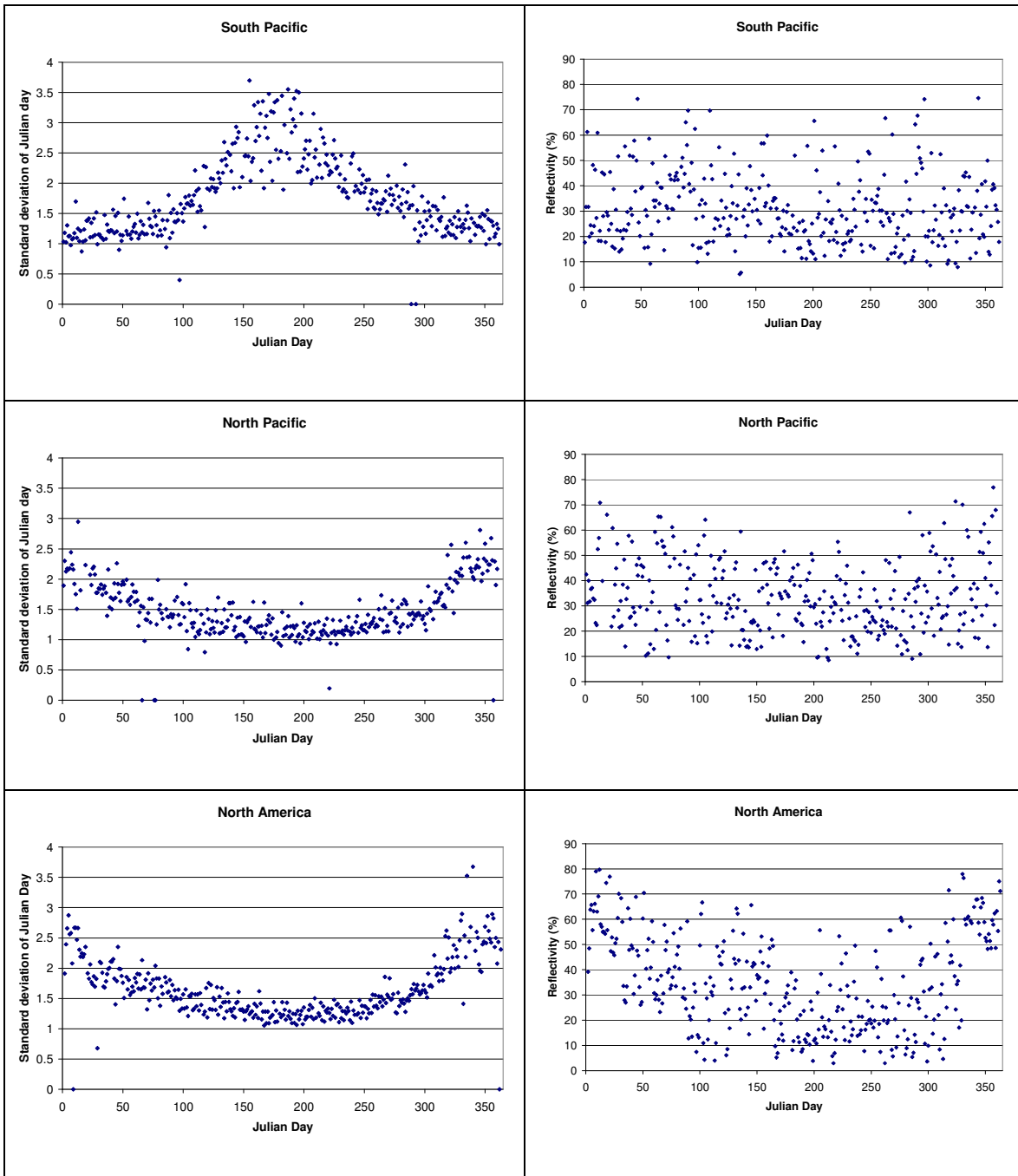


Figure 8: The left hand column shows the standard deviation of each day versus its corresponding Julian day for all three clean regions. The right hand column is the average reflectivity for each box per day versus the corresponding Julian day for all three clean regions.

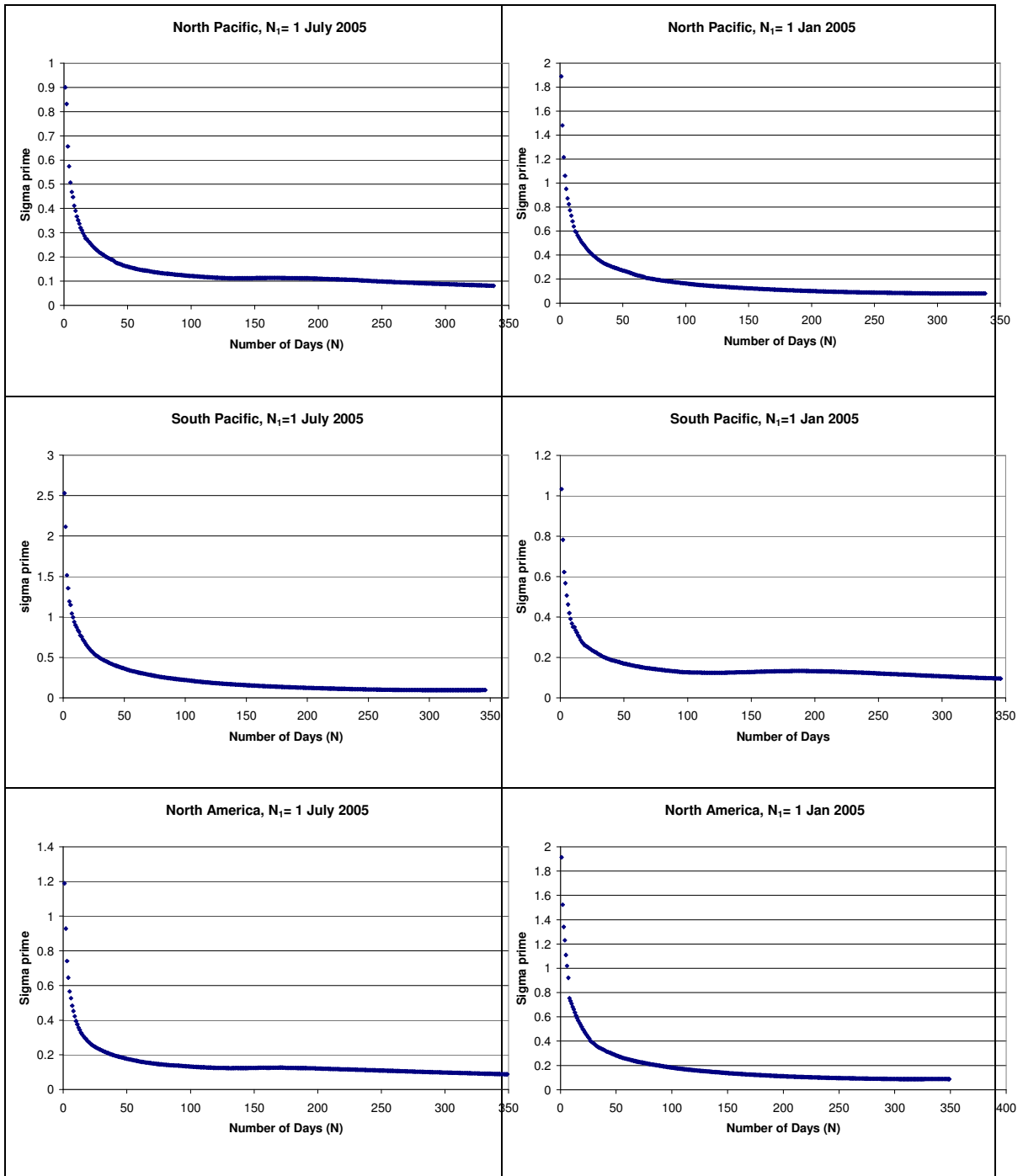


Figure 9: Sigma prime versus the number of days in 2005 over the three clean regions. Sigma prime is equal to the average standard deviation divided by the square root of the number of measurements, N . In the left hand column $N_1 = 1$ July 2005 and the right hand column has $N_1 = 1$ January 2005. Note the seasonal dependence of the graphs.

Location	Spring (DU)	Summer (DU)	Fall (DU)	Winter (DU)
S. Pacific	-0.2 (0.6)	0.1 (0.3)	0.0 (0.4)	-0.4 (0.8)
N. Pacific	-0.2 (0.7)	-0.1 (0.6)	0.1 (0.5)	-0.3 (0.7)
N. America	-0.3 (0.8)	0.1 (0.5)	0.1 (0.6)	-0.2 (0.6)

Table 4a: Seasonal average SO₂ column contents for three regions in 2005. The latitude and longitudes for the regions are as follows: N. Pacific [41 43°N, 130 140°W], S. Pacific [40 44°S, 128 134°E], and N. America [40 50°N, 90 100°W]. In the northern hemisphere spring was considered to be March-May, summer: June-August, fall: September-November, winter: December-February. These months were reversed for the southern hemisphere (ie. Winter: June-August). The standard deviation is shown in parenthesis.

3.5 Conclusions

The yearly mean SO₂ values from the BRD algorithm over all three regions (Table 4) are -0.1 DU. This consistency seems promising for the precision and accuracy of the BRD algorithm over long time periods. The distribution around this mean is nearly constant at a standard deviation of 0.6 DU. The kurtosis of all of these values is greater than 0, suggesting the noise is not normally distributed but is more peaked. This consistency of negative mean values over land and water for long time periods suggests that the BRD algorithm has a slightly negative bias of -0.1 DU. Figure 9 shows that the noise of the OMI BRD algorithm retrieval scales well with the square root of N up to about 100 days independent of the starting time of the year. Depending on the season chosen as the starting day a peak may or may not be seen after ~100 days. Using time averaging the uncertainty, defined as 2 sigma, can be reduced to 0.2 DU or 1 ppb in a 2 km thick layer. This is promising for future work in regions where the seasonal average SO₂ is a few ppb such as over the Eastern seaboard of the United States. Averaging over longer than 100 days does not improve the detection limit.

Breaking down the three regions into seasons shows an interesting trend. In the months where reflectivity is higher (Figure 8) due to snow and ice cover (winter and spring), all three regions have negative mean values and larger standard deviations than the summer and fall (Table 4a). Over North America the noise of the system is the lowest during the summer when the albedo is the lowest. All three regions have lower standard deviations during their summer months when the reflectivity is lowered (Figure 8). This may also be due to lower ozone loading in the summer or other column content feature changes between the seasons. The BRD algorithm has a small negative bias during the winter and spring, -0.3 DU and -0.2 DU respectively, but no bias in the summer and spring. This bias may be caused by changes in reflectivity, temperature, ozone and aerosol loading, or other changes in atmospheric chemical composition. The cause of the bias is still under investigation.

Comparison of the noise in the different algorithms is more difficult due to the small range of Spectral Fit data currently available. Only ten-day averages can be used for this analysis. The BRD algorithm for this small sampling period hovers around zero in all three regions though it does not show the consistency of the long-term data resulting in larger uncertainty. All three algorithms resulted in a negative mean agreeing with the spring time negative bias seen in Table 4a. The SF data in these regions is consistently slightly negative by ~ -0.1 DU on average. If this result is steady over longer time scales, the negative bias of the Spectral Fit algorithm is similar to that of the BRD algorithm. Also, the values found by the Spectral Fit algorithm in the three different regions are more constant than the BRD algorithm. The combined BRD & SF algorithm is the most negative of the three with a bias of ~ -0.25 DU. All three algorithms are

within the standard deviation of the other algorithms which shows their precision. The consistency of all three algorithms to result in slightly negative values over a short time periods and long time periods for the BRD algorithm may also suggest that the OMT03 data used to determine the SO₂ loading may be the cause of these negative results.

CHAPTER 4: Validation Study

A validation study was completed for 1, 5, 7, and 10 April 2005. Aircraft measurements have been compared with OMI measurements using the various algorithms as described in Chapter 2. The $2^{\circ} \times 2^{\circ}$ sampling region is over Eastern China [122 124°E, 41 43°N] and the AMF is 0.36 unless otherwise noted for all calculations. The meteorology of the dates is also analyzed to determine source regions and aerosol loading.

4.1 1 April 2005

Hysplit (Draxler et al., 2003) back trajectories on 1 April 2005 show air in the sampling region coming from the North and Northwest (Figure 11), a region with few SO₂ sources. A few large cities, including Shenyang and Fuschun, lie due north of the sampling region. These cities have been previously shown to have high SO₂ emissions (Streets et al., 2003). Measurements of this region showed significant SO₂ both from the OMI and the aircraft measurements. The BRD algorithm has the highest retrieval (2.1 ± 1.5 DU) and the SF & BRD algorithm had the lowest (0.9 ± 1.0 DU). The aircraft and SF algorithm has similar results, 1.3 ± 0.2 DU and 1.1 ± 1.0 DU respectively (Figure 10). The aircraft only completed one spiral on this date above the Taoxian Airport.

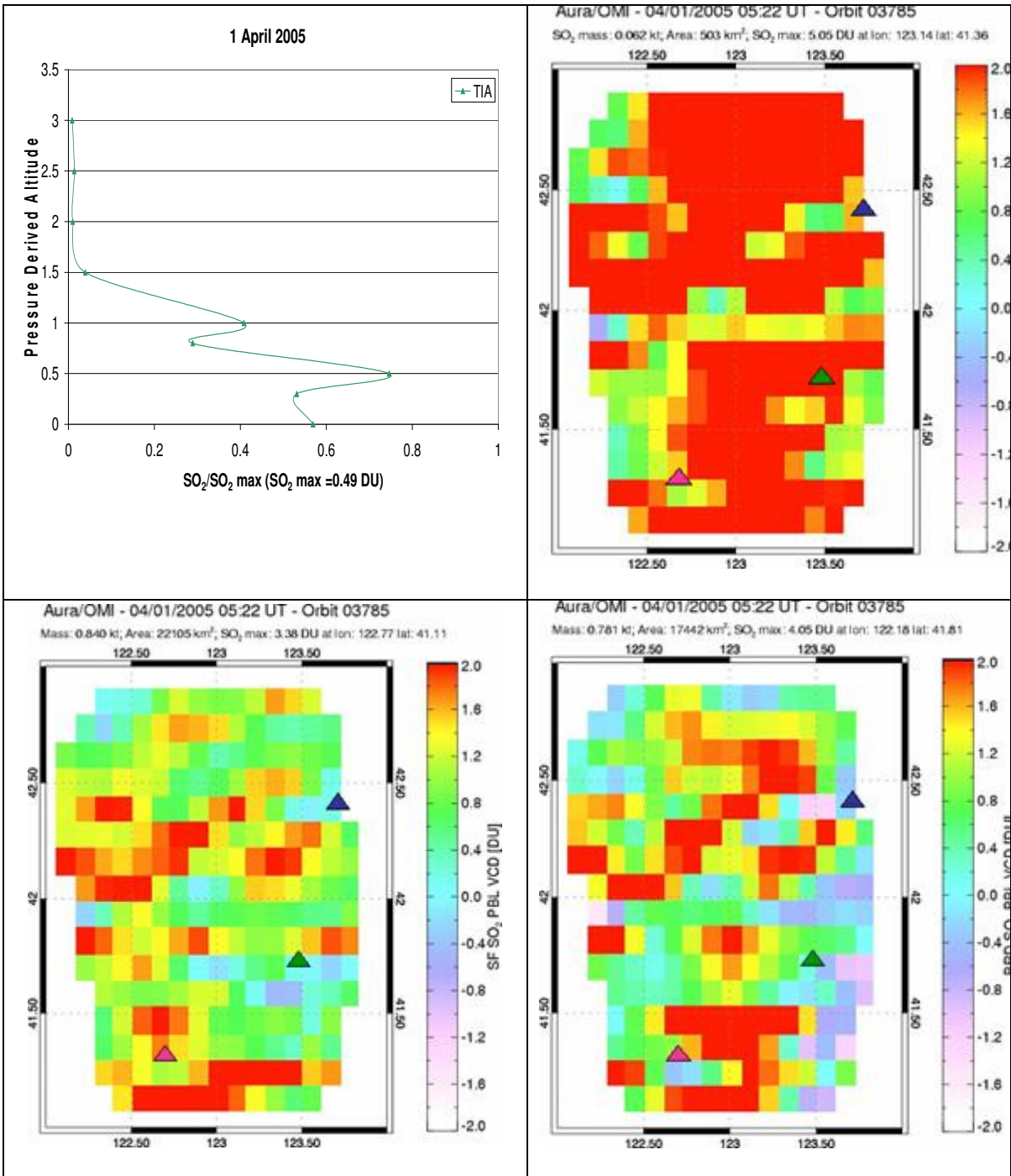
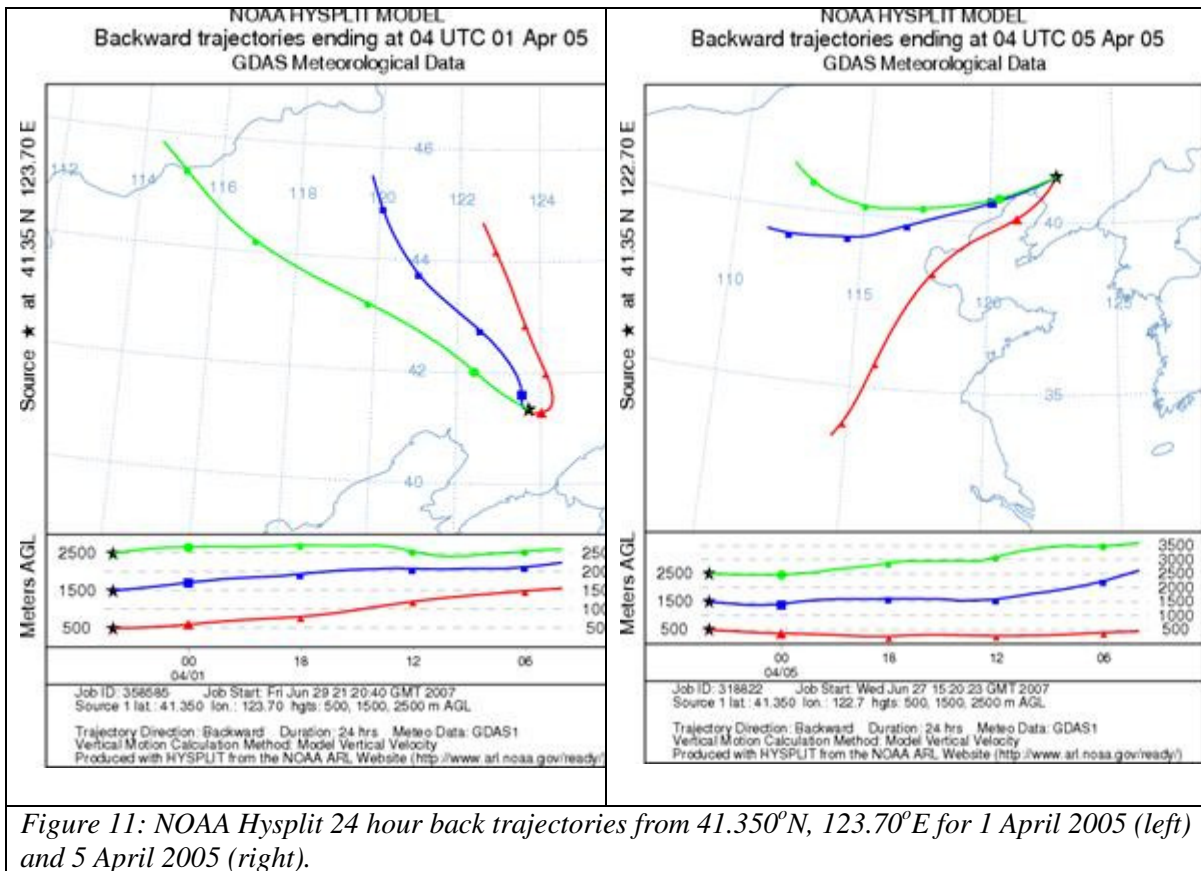


Figure 10: Top left: Normalized aircraft profile from 0-3km over Taoxian Airport on 1 April 2005 using the maximum values from all flights. Top right: BRD algorithm retrieval for 122 124°E, 41 43°N on 1 April 2005. Bottom Left: SF algorithm retrieval for 122 124°E, 41 43°N on 1 April 2005. Bottom Right: SF&BRD algorithm retrieval for 122 124°E, 41 43°N on 1 April 2005. The triangles show the spiral locations. The pink, Liaozhung, the green, Taoxian Airport, and the blue, Xiaoming.



4.2 5 April 2005

On 5 April 2005 air originated from the southwest into the sampling region (Figure 11) ahead of a cold front. As the air passed over the eastern coast of China it passed many SO₂ sources allowing the air to accumulate SO₂. The air also picked up many anthropogenic aerosols such as black carbon. Figure 12 shows the SO₂ loading determined by the aircraft at three locations (as described in Section 1.1) and OMI retrievals for the BRD, SF, and SF&BRD algorithms.

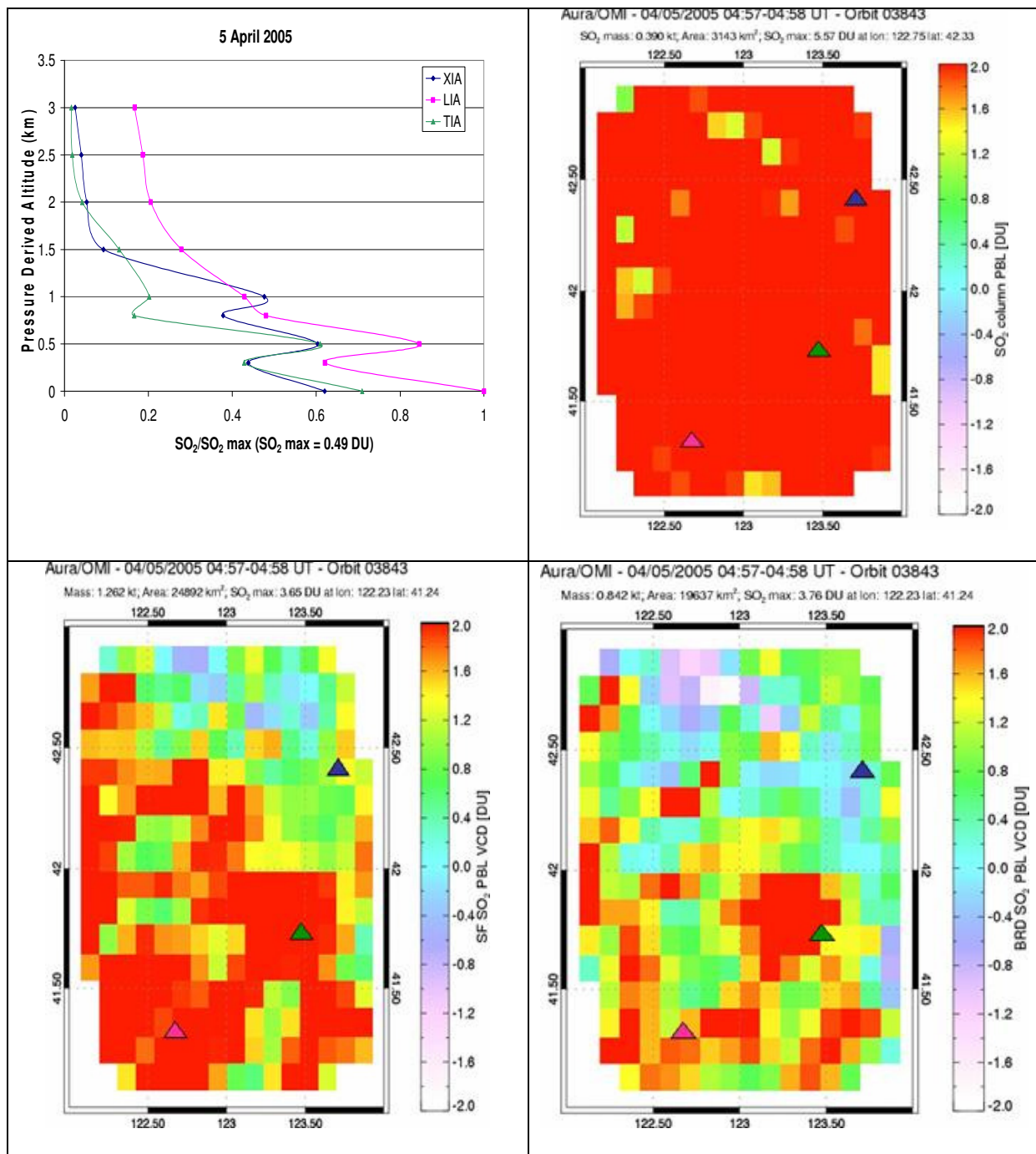


Figure 12: Top left: Normalized aircraft profile from 0-3km over the three spiral locations on 5 April 2005 using the maximum values from all flights. Top right: BRD algorithm retrieval for 122 124°E, 41 43°N on 5 April 2005. Bottom Left: : SF algorithm retrieval for 122 124°E, 41 43°N on 5 April 2005. Bottom Right: : SF & BRD algorithm retrieval for 122 124°E, 41 43°N on 5 April 2005. The triangles show the spiral locations. The pink, Liaozhung, the green, Taoxian Airport, and the blue, Xiaoming.

The AMF was modified on 5 April using the SO₂ profiles seen with the aircraft

(Figure 8) and the aerosol loading determined by the aircraft. The aircraft measured an

aerosol index of about 2.1. Correcting the SO₂ values for 5 April results in increased SO₂ loading (2.8 DU) over Xiaoming and Liaozhung, making the airplane and OMI BRD retrieval agreement decrease.

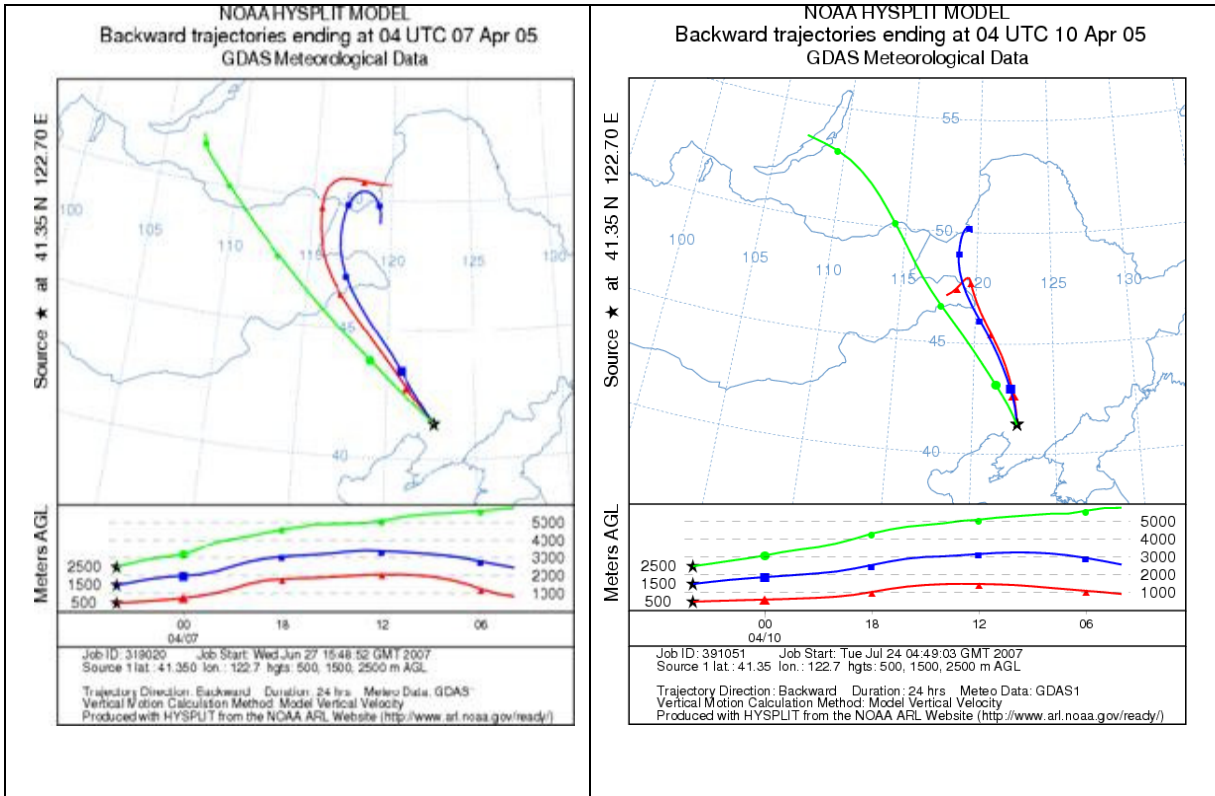


Figure 13: NOAA Hysplit 24 hour back trajectories from 41.350°N, 123.70°E for 7 April 2005 (left) and 10 April 2005 (right).

4.3 7 April 2005

The air mass in the sampling region moved in from the northwest after the cold front passed through the region on 6 April (Figure 13). This front “cleaned out” the air, leaving little SO₂ and industrial aerosols. The air did not pass over any regions of known SO₂ emission and carried with it mineral dust from the Mongolian desert region. Figure 14 shows the SO₂ profile from the aircraft and OMI retrievals for the same area.

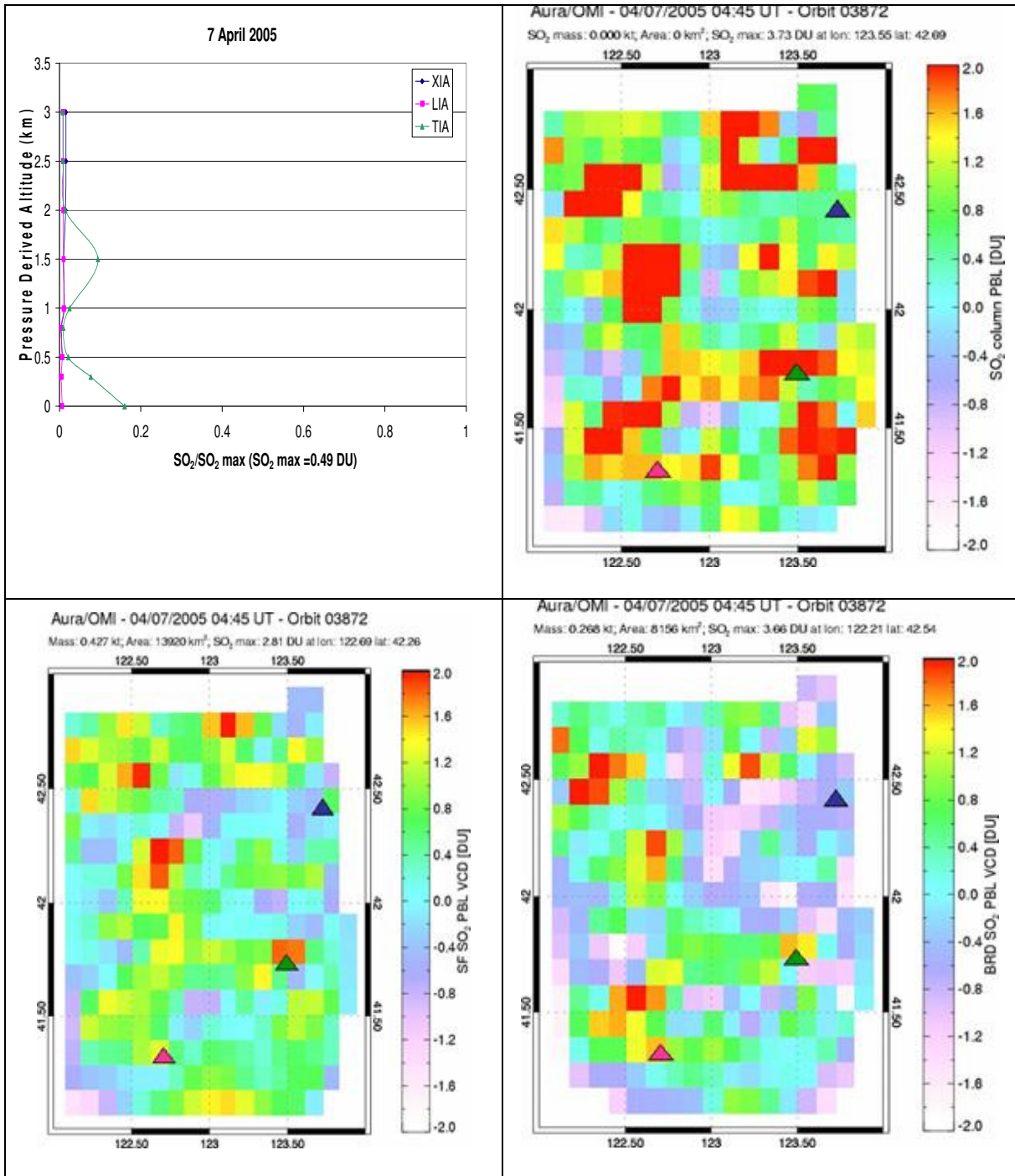


Figure 14: Top left: Normalized aircraft profile from 0-3km over the three spiral locations on 7 April 2005 using the maximum values from all flights. Top right: BRD algorithm retrieval for 122 124°E, 41 43°N on 7 April 2005. Bottom Left: : SF algorithm retrieval for 122 124°E, 41 43°N on 7 April 2005. Bottom Right: : SF & BRD algorithm retrieval for 122 124°E, 41 43°N on 7 April 2005. The triangles show the spiral locations. The pink, Liaozhung, the green, Taoxian Airport, and the blue, Xiaoming.

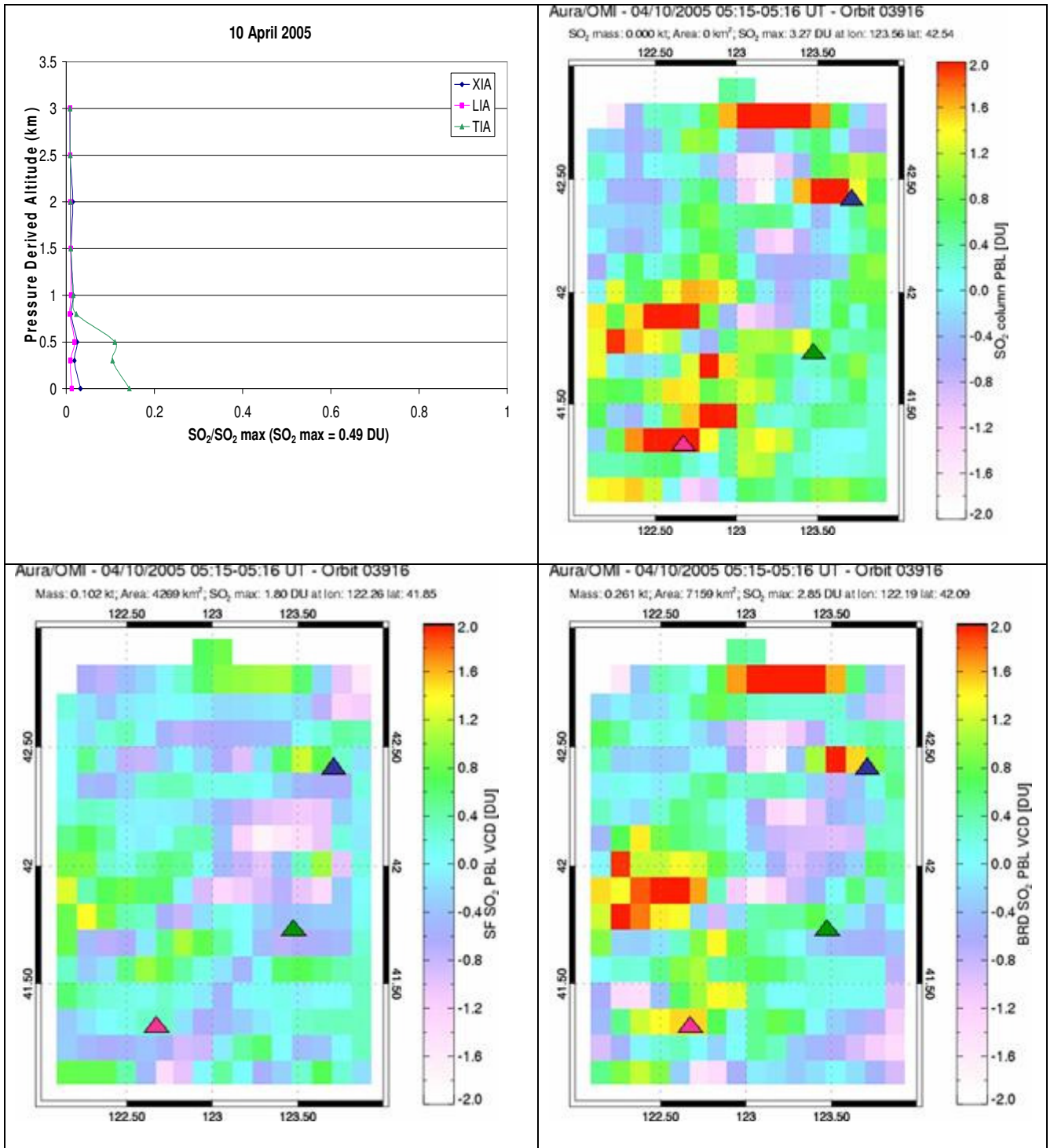


Figure 15: Top left: Normalized aircraft profile from 0-3km over the three spiral locations on 10 April 2005 using the maximum values from all flights. Top right: BRD algorithm retrieval for 122 124°E, 41 43°N on 10 April 2005. Bottom Left: : SF algorithm retrieval for 122 124°E, 41 43°N on 10 April 2005. Bottom Right: SF & BRD algorithm retrieval for 122 124°E, 41 43°N on 10 April 2005. The triangles show the spiral locations. The pink, Liaozhung, the green, Taoxian Airport, and the blue, Xiaoming.

4.4 10 April 2005

Hysplit trajectories for 10 April show a similar condition as seen on 7 April (Figure 13). The air had low SO₂ loading because it passed over few SO₂ emission sources, as may be seen by both aircraft measurement and OMI retrievals (Figure 15).

4.5 Comparisons and Discussion

Mean SO₂ values and standard deviations are shown in Table 5. The BRD algorithm yields numbers that are higher than airplane measurements for all days

	1 April (DU)	5 April (DU)	7 April (DU)	10 April (DU)
<i>SF</i>	1.09 (0.95)	1.60 (1.00)	0.44 (1.24)	-0.058 (0.81)
<i>(SF+BRD)</i>	0.87 (1.50)	0.99 (1.17)	-0.050 (1.24)	0.14 (1.16)
<i>BRD</i>	2.07 (1.45)	2.87 (1.15)	0.90 (1.40)	0.45 (1.18)
<i>Airplane average</i>	1.3 (0.2)	1.6 (0.3)	0.10 (0.02)	0.09 (0.01)

Table 5: Column contents of SO₂ over 41 43° N, 122 124° E with the standard deviation in parenthesis for all three algorithms and average aircraft retrieval.

sampled. This suggests that the SO₂ between sampling regions may have been higher.

Looking at the detailed pictures of the OMI BRD retrieval show that pixels between the sampling region are higher making this a reasonable assumption though it likely does not account for the entire discrepancy. The percent difference between the aircraft and the OMI values was determined using the equation

$$\% \text{ difference} = \frac{\text{airplane (DU)} - \text{OMI (DU)}}{\text{airplane (DU)}} \times 100\% \quad (5)$$

	1 April (% difference)	5 April (% difference)	7 April (% difference)	10 April (% difference)
Airplane: SF	16	0	340	164
Airplane: SF&BRD	33	38	-150	-56
Airplane: BRD	-59	-79	-800	-400

Table 6: The percent difference between the in situ airplane data and the various algorithms calculated using equation 5.

The results of equation 5 are given in Table 6.

All three algorithms have a much better agreement with airplane measurements when the SO₂ loading is greater than 1.0 DU, to forthwith be called “high loading”. The Spectral Fit data has the best agreement when there is high loading. In low loading situations, SO₂ less than 0.5 DU, all three algorithms accuracy decrease. The OMI is able to distinguish between high and low SO₂ loading on a daily basis. Currently, the quantitative results have large uncertainties making numerical analysis less reliable than qualitative analysis. The ability to distinguish on a daily basis between high and low SO₂ loading is novel among satellites.

CHAPTER 5: Trajectory Analysis

The SO₂ plume observed on 5 April 2005 was followed for three days to determine whether the OMI was able to track plume movement and to estimate the lifetime of SO₂. All values were calculated using the BRD algorithm with AMF corrections. The Corrections were determined from observed aircraft profile and aerosol height.

5.1 Forward trajectories of the polluted air

Three daily, 24-hour trajectories were used to verify a 72-hour forward air mass trajectory starting on 5 April 2005, 18:00 UTC. Trajectory simulations were made using the NOAA HYSPLIT model. A box was made around the plume seen on 5 April 2005 (Figure 15) and the four corners were used as the starting latitude and longitude points for the forward trajectories. Each trajectory was made for a 24-hour time period to determine the new location of the air mass on a daily basis. This new location was used as a starting position for another 24-hour trajectory. Finally, a third 24-hour trajectory was modeled using the previous 24-hour trajectory's end point. These three 24-hour trajectories were concatenated and compared to the 72-hour trajectory (Figure 16c). This data showed that the final locations of both the three 24 hour trajectories and the 72-hour trajectory were in agreement.

During the trajectory simulations, altitudes of the mass of pollution were also taken into consideration. Based on aircraft data, all of the significant SO₂ mass on 5 April 2005 was determined to be between 0-3 km, with the majority concentrated below 2km. Subsequently, only air from this region was considered to contain SO₂ and used in further calculations. The forward trajectories of this air mass to 6 April were then used to

determine the maximum and minimum heights of SO₂ for the following day. This process was repeated for 7, 8 April. These heights are given in Table 7.

5.2 Plume Trajectory, 5-8 April 2005

The 35 49°N, 117 132°E box under consideration on 5 April 2005 was followed until 8 April 2005 when the plume became very dispersed. The air mass was assumed to move along as predicted by Hysplit forward trajectories as described above. This was confirmed by the OMI data which showed the plume moving east each day along the same path. The plume showed significant rising of the air that originated between 0-3 km above ground from 5-6 April as the air moved out to sea. The mechanism for lofting has been suggested to be WCB (Dickerson et al., 2007). The air height then remained nearly constant between 2-5 km until the air mass became too spread out and diluted with other air to have a clear plume anymore. A corrected AMF (Figure 14d) was used to calculate the mass of SO₂ for 6-8 April 2005 due to this lofting. The corrected AMF assumed the SO₂ had a Gaussian profile around 3km. The sensitivity of the OMI detection increases directly with SO₂'s atmospheric height. Therefore, without making a correction for the lofting, the amount of SO₂ increased, appearing to violate conservation of mass (Figures 16a and 16b). This is demonstrated between 5 and 6 April in Table 7. Using air mass trajectories, SO₂ height may be determined and an appropriate AMF correction applied to the data. OMI offers the unprecedented ability to track SO₂ movement for high loading

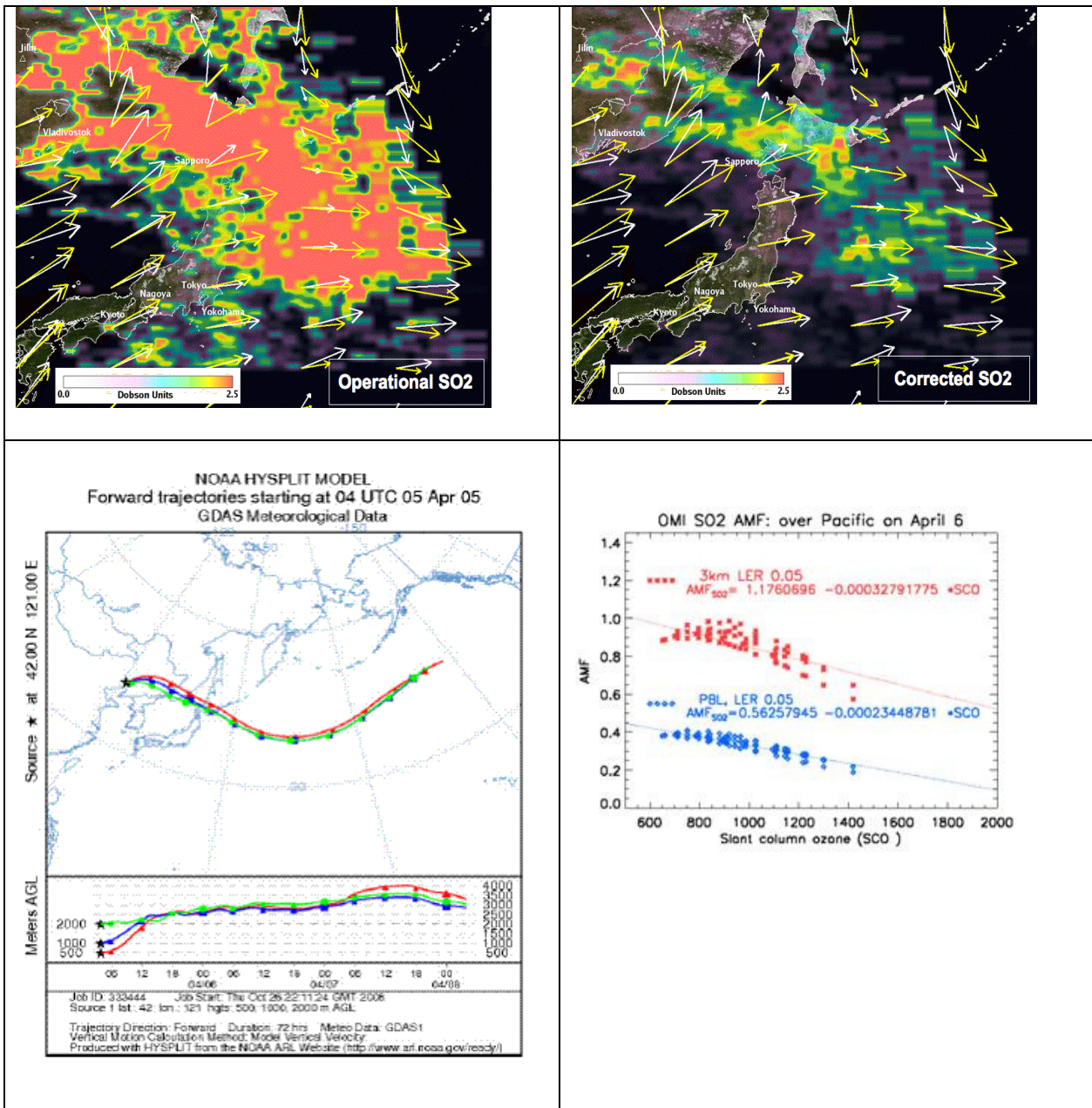


Figure 16 (a-top left): OMI operational PBL SO₂ on 6 April 2005. The amount of SO₂ is overestimated due to the SO₂ height being above the algorithm. (b-top right) OMI SO₂ data corrected for the elevated plume altitude (~3km) and reflectivity. (c-bottom left) NOAA Hysplit trajectory originating at 42N, 121E on 5 April 05 at 4 UTC for 500, 1000, and 2000m air. The trajectory illustrates the air being lofted up to 3000m rapidly as it heads out to sea and remaining at that height during transport over the Pacific Ocean. Similar trajectories were seen from other points located within the sampling region. (d-bottom right) AMF regressions for PBL plume and elevated plume ~3km on 6 April. As the AMF increases the amount of SO₂ in the column will decrease.

episodes. Figure 17 shows OMI retrieval from 5-8 April using the corrected AMFs with

boxes around the sampling mass region.

Date	Minimum Height (km)	Maximum Height (km)
5 April 2005	0.0	3.0
6 April 2005	2.0	4.0
7 April 2005	3.0	5.0
8 April 2005	2.0	5.0

Table 7: The maximum and minimum height of SO₂ loading for each day as determined from aircraft measurements and air mass trajectories.

5.3 SO₂ mass calculations

SO₂ mass was calculated on 5 April 2005 assuming the SO₂ is concentrated below 3 km. For 6-8 April, the SO₂ mass was determined by assuming the SO₂ had a Gaussian profile around 3 km. This correction was made to account for the lofting determined from the trajectory analysis discussed above. The box size was kept constant assuming no SO₂ dispersion.

Date	SO ₂ (AMF=PBL) (tonnes)	SO ₂ (AMF=3km Gaussian) (tonnes)	Box size (km ²)
5 April 2005	74600	---	1950000
6 April 2005	76400	32600	1950000
7 April 2005	31800	13200	1940000
8 April 2005	32200	10100	2080000

Table 8: OMI SO₂ masses for each day calculated using the standard AMF in the OMSO₂ product and using a corrected AMF assuming the SO₂ has a Gaussian distribution around 3km.

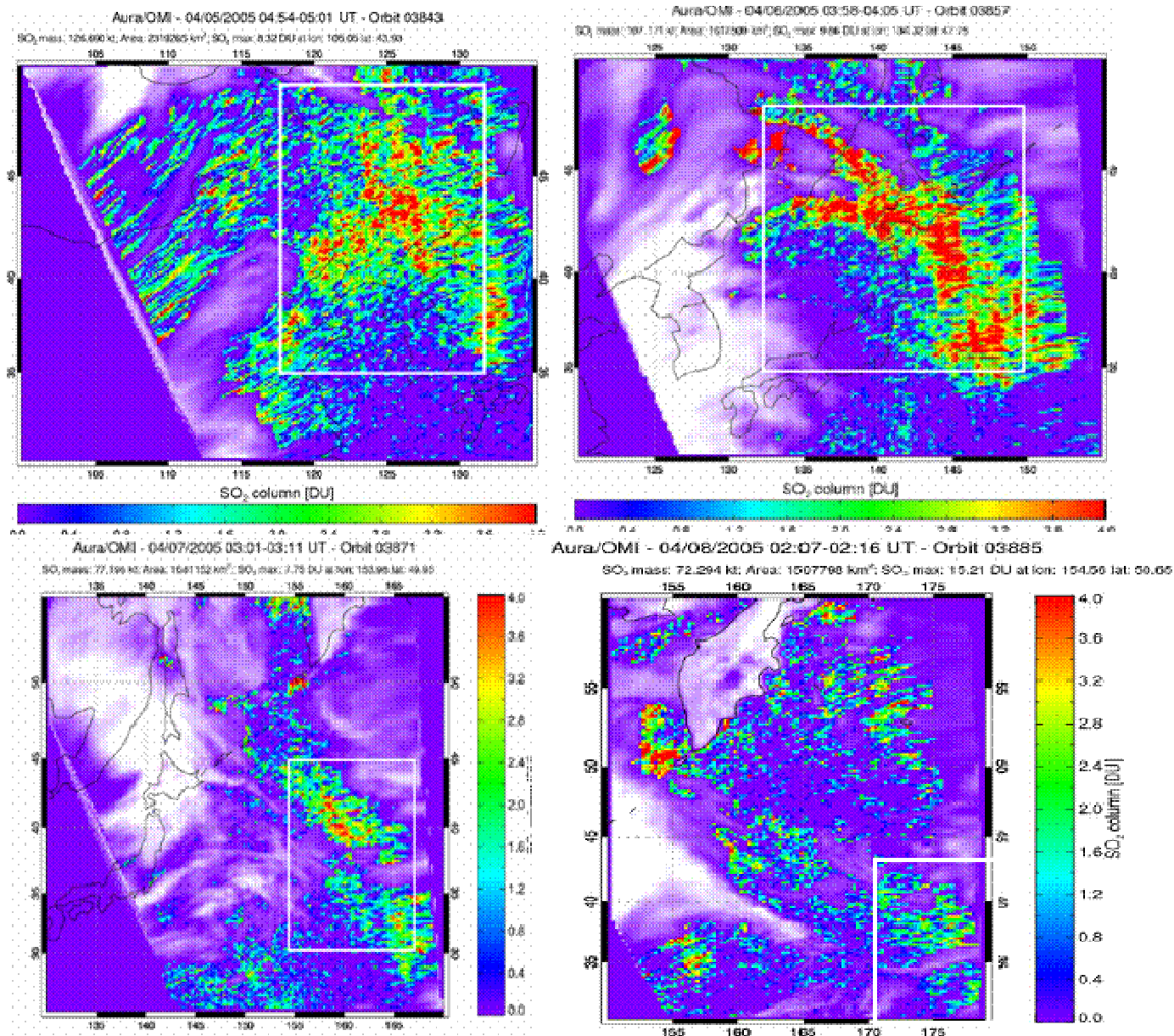


Figure 17: SO₂ plume motion from 5 April (top left) to 8 April (bottom right). The area of the plume measured is shown by the white box. Note the longitude of the plots change as the plume moves eastward.

5.3 Lifetime and Dispersion

The initial SO₂ plume on 5 April 2005 traveled east over the sea of Japan on 6 April 2005 after being lofted above 2 km. Trajectory analysis shows that the majority of

the plume followed this path but some of it traveled north, away from the main pathway. Based on trajectories about 30% of the initial SO₂ plume did not travel with the plume over the Sea of Japan on 6 April (Li, C. et al, 2007). In determining the SO₂ mass, the OMSO₂ product uses a background box correction to account for background levels of SO₂. These boxes change the mass of SO₂ by 35% on average but can have both larger and smaller effects (Table 9). Therefore, a 35% uncertainty is expected with the mass measurements.

Trial	Minimum Latitude (N)	Minimum Longitude (E)	Maximum Latitude(N)	Maximum Longitude (E)	Area (km ²)	Background Box SO ₂ (tonnes)	Total SO ₂ (tonnes)	Uncertainty percentage
standard	50	105	55	110	194166	0	76584	0.00
1	20	135	25	140	294725	11726	64857	15.31
2	35	120	40	125	253069	49194	27389	64.24
3	45	115	50	120	215490	33184	43400	43.33
4	45	130	50	135	215490	42582	34001	55.60
5	45	105	50	110	215490	2967	73616	3.87
6	45	105	55	120	1210058	11455	65128	14.96
7	52	105	55	107	49537	0	76584	0.00
8	45	105	55	125	1610308	23875	52708	31.17
9	40	110	50	120	890906	33227	43356	43.39
10	30	105	55	135	6837127	33175	43408	43.32
11	25	105	55	140	9880410	20001	56582	26.12

Table 9: SO₂ mass calculations for the box (35 49°N, 117 132°E) on 5 April 2005. The standard was used as the basis for background box size and locations. Trials 1-5 have similar areas but the locations and SO₂ loading varying substantially. Trials 6-11 have varying background box areas but are all in the same locations. This yields background boxes with more consistent masses.

Taking both of these errors into account the lifetime of SO₂ from this trajectory analysis ranges from 1.0 to 3.0 days (Figure 18).

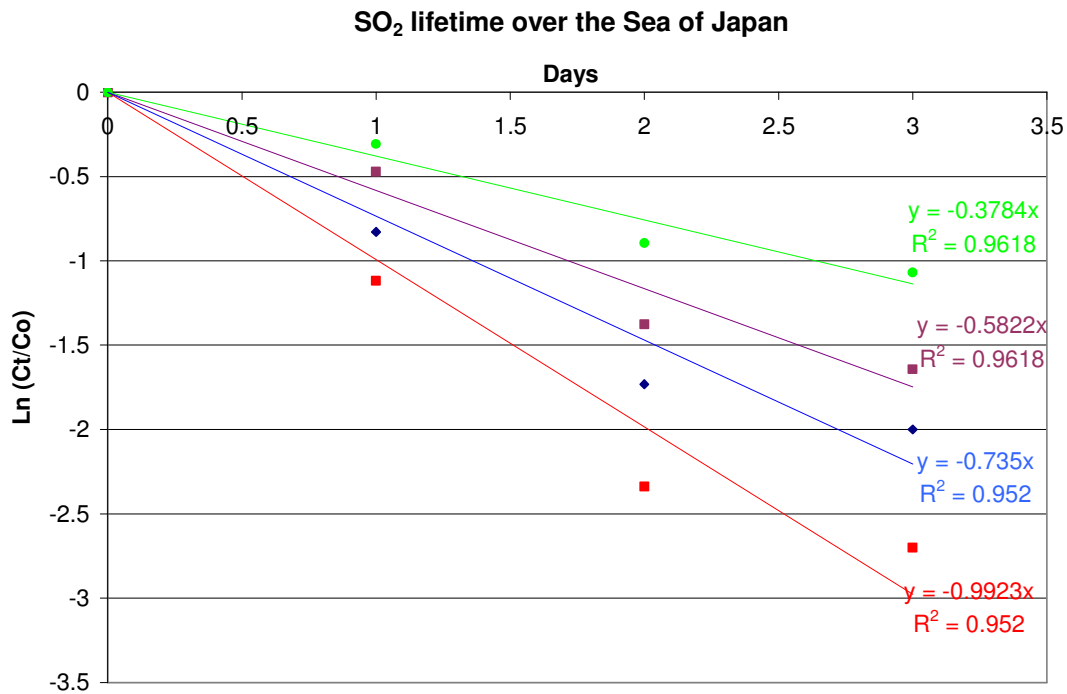


Figure 16: SO₂ lifetime over the Sea of Japan as an SO₂ plume from 5 April 2005 travels eastward over the Sea of Japan to the Atlantic. The blue line shows the average SO₂ mass changes due to lofting, neglecting dispersion. The purple is the average SO₂ mass assuming 30% dispersion from 5-6 April. The red represents the highest SO₂ loading with uncertainty and corresponds to a lifetime of ~1 day. The green is the lowest SO₂ loading (assuming 30% lost to dispersion and 35% uncertainty in the measurements) and corresponds to a lifetime of ~3 days.

5.4 Conclusions

Using tools available online and the OMSO₂ product, the path of SO₂ released into the PBL can be tracked. This novel ability will prove useful for determining the extent of SO₂'s impact as it travels in the atmosphere. This study revealed a lifetime of ~1-3 days. This is within previous estimates of lifetime as discussed in the introduction. Overall, OMI shows promise in its ability to track SO₂ in the PBL for a few days, though dispersion limits the length of this tracking ability. A rough lifetime has been estimated though this will improve with improved SO₂ retrieval from the OMI.

CHAPTER 6: Discussion

The OMI has the ability to see on a daily scale the difference between high and low SO₂ vertical column contents using all three algorithms. Currently, the SF algorithm shows the best agreement with *in situ* data over China, with less than 15% difference on high-loading days. The BRD algorithm is precise but it is not highly accurate (~ 40% difference) on high-loading days. Combining the two algorithms decreases both the accuracy and precision for all loadings. On low-loading days, all three of the algorithms fail to have precise measurements with percentage errors greater than 100. This is most likely due to the SO₂ levels being below the detection limit of the instrument.

As the time scale increases so too does the accuracy and precision of the OMI's measurement. Three six-month averages (January-June) of the BRD algorithm over clean regions in 2005 lead to mean values that ranging from -0.3 to 0.1 DU, yet when the time scale is increased to a year for the same regions, the algorithm yields -0.1 DU for the North Pacific, South Pacific, and North American clean regions (Chapter 3). The standard deviation of the mean is 0.6, 0.7, and 0.6 DU respectively leading to an average standard deviation of mean 0.6 DU. Yet this does not accurately describe the SO₂ concentrations in these regions as seasonal variations are ignored and accuracy decreases. In the winter and spring of 2005, all three regions have negative mean values and standard deviations between 0.6-0.8 DU yet in the summer and fall the mean values are within 0.1 DU of zero and the standard deviations decrease to 0.3-0.5 DU. The noise scales with the square root of N up to ~ 100 days. Averaging over longer time periods does not improve the detection limit due to seasonal variations.

The OMI is also able to track SO₂ plumes for a period of days, offering novel information to the scientific community. Tracking the motion of SO₂ once released will enable improved SO₂ lifetime in models and help determine the impact of a source region on a global scale. In this analysis, a lifetime of 1 to 3 days was determined though this may change with more accurate mass estimates in the future.

CHAPTER 7: Future Work

- 1) The Spectral Fit data needs to be expanded so that longer time periods and more scenarios may be studied using the SF algorithm. This would lead to a better understanding of the uncertainty associated with this algorithm. Currently this algorithm requires manual determination of the residuals making it time-consuming and unrealistic for use with all incoming data from the OMI. Determining an algorithm to compute these residuals is essential to make the SF algorithm a viable retrieval option.
- 2) The current AMF correction for the BRD algorithm seems to increase the column loading and decrease the agreement with the *in situ* data. Better AMF correction could help improve BRD algorithm's accuracy. More work is needed to determine how to enhance the AMF to improve the retrieval. Current AMF corrections do not incorporate *in situ* ozone corrections which could help improve them.
- 3) OMI data needs to be compared with model studies with SO₂. This will allow analysis of longer time periods than *in situ* data provides. One future plan is to compare OMI data with SO₂ from the GO-CART model (Chin et al., 2000, Chin et al., 2003).
- 4) More *in situ* data collected via aircraft campaigns would aid in validation studies. Future work includes another flight campaign in China in 2008. The sampling region is southwest of the current campaign, in an area where high SO₂ is seen on a regular basis.
- 5) The OMTO3 data (source data for SO₂) is currently being improved by the algorithm team. Future releases of this data could lead to improved retrieval by one or all of the algorithms discussed. Current analysis was done using Collection 2 data. Preliminary Collection 3 data (due to be released in late summer 2007) shows promising

results over China with the BRD algorithm. Collection 3 data has improved retrieval which minimizes the effect of stray light better than the Collection 2 data. An example of results using the BRD algorithm with the preliminary Collection 3 data is shown in Figure 19b for 1 April 2005.

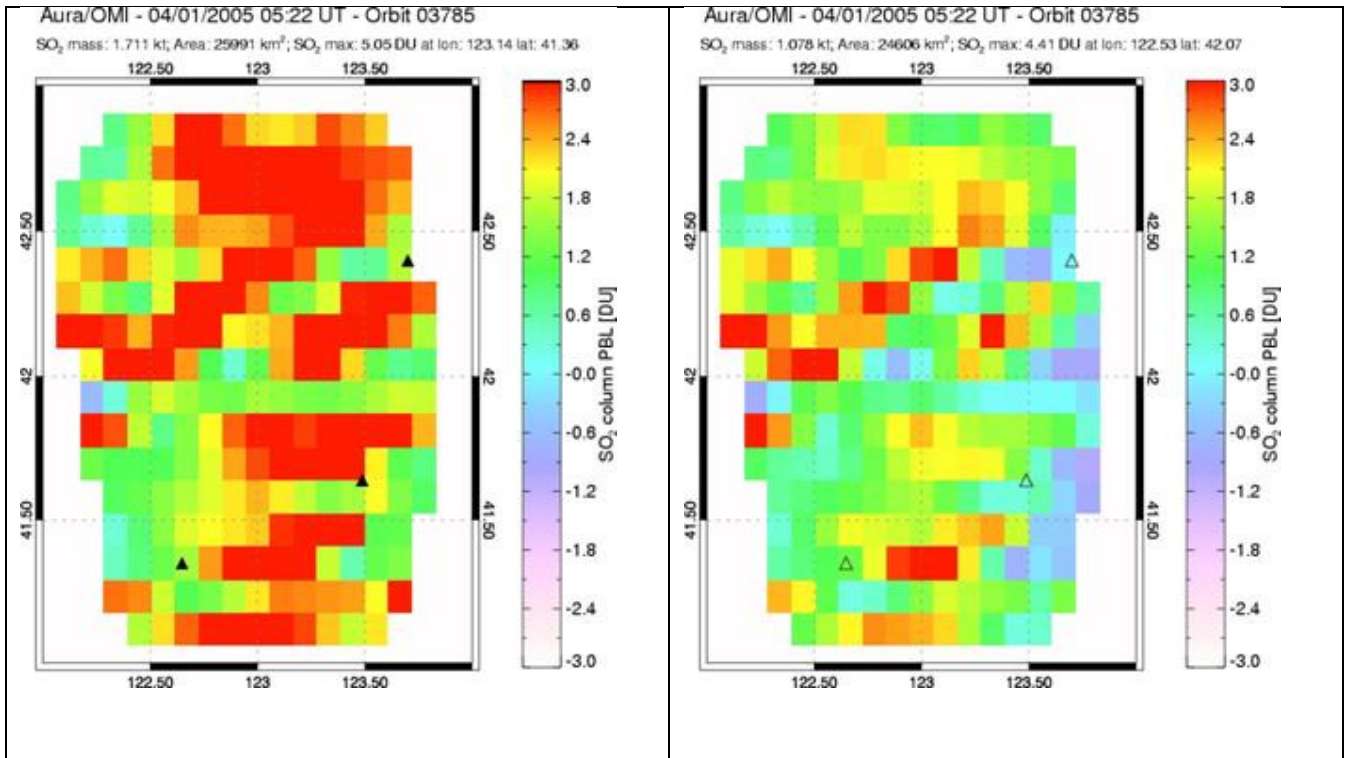


Figure 19a: Collection 2 (OLD)
 Mean SO₂ for region (PBL): 2.072
 SO₂ Std Dev (PBL): 1.445

Figure 19b: Collection 3 (current)
 Mean SO₂ for region (PBL): 1.279
 SO₂ Std Dev (PBL): 1.473

1 April 2005 OMSO2 PBL data (AMF=0.36): Left : Collection 2 (operational) Right: Collection 3 (test data)

The average for the region (1.3 DU) from this retrieval matches the aircraft-measured value in this region of 1.3 DU. Future examinations with Collection 3 data are necessary once the information is publicly released.

WORKS CITED

- Benkovitz, C.M., Schwartz, S. E., Jensen, M. P., and Miller, M. A. (2006) "Atmospheric Chemistry and Physics Discussions Attribution of Modeled Atmospheric Sulfate and SO₂ in the Northern Hemisphere for June–July 1997". Atmos. Chem. Phys. Discuss. **6**, 4023–4059.
- Berglen, T.F., Berntsen, T.K., Isaksen, S.A., Sundet, J.K., (2004). "A global model of the coupled sulfur/oxidant chemistry in the troposphere: The sulfur cycle", J. Geophys. Res. **109**, D19310, doi:10.1029/2003JD003948
- Bhartia, P. K. and C. W. Wellemeyer (2002), OMI TOMS-V8 Total O3 Algorithm, Algorithm Theoretical Baseline Document: OMI Ozone Products, edited by P K. Bhartia, vol. II, ATBD-OMI-02, version 2.0. Available: http://eosps0.gsfc.nasa.gov/eos_homepage/for_scientists/atbd/docs/OMI/ATBD-OMI-02.pdf
- Bogumil K, Orphal J, Homann T, et al. (2003). "Measurements of molecular absorption spectra with the SCIAMACHY pre-flight model: instrument characterization and reference data for atmospheric remote-sensing in the 230-2380 nm region" Journal of Photochemistry and Photobiology A-Chemistry **(2-3)**: 167-184.
- Bovensmann, H., et al. (1999). "SCIAMACHY-Mission objectives and measurement modes." J. Atmos. Science **56**: 127-150.
- Burrows, J. P., Weber, M., Buchwitz, V., Rozanov, Ladstatter-Weisenmayer, A., Richter, A., de Beek, R., Hoogen, R., Bramstedt, K., Eichmann, K. U., Eisenger, M., Perner, D. (1999). "The Global Ozone Monitoring Experiment (GOME): Mission Concept and first scientific results." J. Atmos. Science **56**: 151-175.
- Chin, M., P. Ginoux, et al. (2003). "A global aerosol model forecast for the ACE-Asia field experiment." Journal of Geophysical Research-Atmospheres **108**(D23).
- Chin, M., D. L. Savoie, et al. (2000). "Atmospheric sulfur cycle simulated in the global model GOCART: Comparison with field observations and regional budgets." Journal of Geophysical Research-Atmospheres **105**(D20): 24689-24712.
- Chin, M., D. J. Jacob, G. M. Gardner, M. S. Foreman-Fowler, P. A. Spiro, and D. L. Savoie (1996), "A global three-dimensional model of tropospheric sulfate", J. Geophys. Res., **101**(18)667–18,690
- Cullis, C. F., Hirschler, M.M: Atmospheric Sulfur- Natural and Man-made sources. Atmospheric Environment **14**(11): 1263 (1980).

- Dickerson, R. R. et al. (2006). "Aircraft observations of dust and pollutants over NE China: Insight into the meteorological mechanisms of long-range transport", Submitted Journal of Geophysical Research-Atmospheres.
- Dobbler, M.R., Dirksen, R.J. et al, (2006) "Ozone Monitoring Instrument Calibration." IEEE transaction of Geoscience and Remote Sensing **44**(5).
- Draxler, R. R., and G.D. Rolph (2003). "HYSPLIT (HYbrid Single-Particle Lagrangian Integrated Trajectory) Model" NOAA ARL READY.
- Edner, H., et al. "Differential Optical-Absorption Spectroscopy (Doas) System for Urban Atmospheric-Pollution Monitoring". Applied Optics **32**(3): 327 (1993).
- Eisinger, M., Burrows, J.P. (1998). "Tropospheric sulfur dioxide observed by the ERS-2 GOME instrument." Geophysical Research Letters **25**: 4177-4180.
- "Eastern China Map." Encyclopedia Britannica Online (2002) Encyclopedia Britannica 10 June 2007 <<http://www.britannica.com>>
- EPA (2007). Six Common Air Pollutants: SO₂. <<http://www.epa.gov/oar/urbanair/so2/>>
- Finlayson-Pitts, B. J., Pitts, J.N. (1976) "Photochemistry of polluted troposphere". Science **192**(4235).
- Gilboa, S. M., Mendola, P., Olshan, A.F., Langlois, P.H., Savitz, D.A. Loomis, D., Herring, A.H., Fixler, D.E (2005). "Relationship between ambient air quality and selected birth defects, seven county study, Texas, 1997-2000". American Journal of Epidemiology **163**(3): 238.
- Gondal, M. A. and Mastromarino, J. (2001) "Pulsed laser photoacoustic detection of SO₂ near 225.7 nm". Applied Optics **40**(12): 2010.
- Guttikunda, S. K., Y. H. Tang, et al. (2005). "Impacts of Asian megacity emissions on regional air quality during spring 2001." Journal of Geophysical Research-Atmospheres **110**(D20).
- Hains, J.C. et al.(2007) "A clustering methodology to identify distinct chemical events in the troposphere using aircraft trace gas and aerosol vertical profiles." manuscript in preparation J.C. Hains.
- Heald, C. L., D. J. Jacob, P. I. Palmer, M. J. Evans, G. W. Sachse, H. B. and a. D. R. B. Singh (2003). "Biomass burning emission inventory with daily resolution: Application to aircraft observations of Asian outflow." J. Geophys. Res. **108**: 8811.

- Honniger, G., Von Friedeburg, C., Platt, U. (2004). "Multi axis differential absorption spectroscopy". Atmospheric Chemistry and Physics 4:231
- Koch, D., D. J. Jacob, I. Tegen, D. Rind, and M. Chin (1999), Tropospheric sulfur simulation and sulfate direct radiative forcing in the Goddard Institute for Space Studies general circulation model, J. Geophys. Res.,104, 23,799– 23,822.
- Krotkov, N. A., S. A. Carn, et al. (2006). "Band residual difference algorithm for retrieval of SO₂ from the aura Ozone Monitoring Instrument (OMI)." Ieee Transactions on Geoscience and Remote Sensing **44**(5): 1259-1266.
- Krotkov, N. A., McClure, B., Dickerson, R.R., Carn, S., Bhartia B.K., Yang, K., Kreuger, A., Li, Z., Hains, J.C., Levelt, P.F., Chen, H., Gong, F., Bian, X.(2007) "OMI SO₂ validation over eastern China using in-situ aircraft measurements". submitted to Journal of Geophysical Research, Special Issue on AURA VALIDATION.
- Kumar, P. C. and Wehrmeyer, J. A. (1997) "Stack gas pollutant detection using laser Raman spectroscopy" Applied Spectroscopy 51(6): 849
- Levelt, P. F., G. H. J. Van den Oord, et al. (2006). "The Ozone Monitoring Instrument." Ieee Transactions on Geoscience and Remote Sensing **44**(5): 1093-1101.
- Li, Can, personal communication, 2007
- C. Li et al. (2007), "Transport and evolution of pollutant plume from East Asia: a case observed from space", manuscript in preparation.Li, C
- Luke, W. T. (1997). "Evaluation of a commercial pulsed fluorescence detector for the measurement of low-level SO₂ concentrations during the Gas-Phase Sulfur Intercomparison Experiment." J. Geophys. Res. **102**: 16255-16265.
- Luo, C., J. C. St. John, X. Zhou, K. S. Lam, T.Wang, and W. L. Chameides (2000). "A nonurban ozone air pollution episode over eastern China: Observations and model simulations." J. Geophys. Res. **105**: 1889-1908.
- Noxon, J. F. (1975) "Nitrogen-dioxide in stratosphere and troposphere measured by ground-based absorption spectroscopy". Science 189(4202): 547
- Noxon, J. F., Norton, R.B., Henderson, W.R.(1978) "Observations of atmospheric N₃" Geophysical Research Letters **5**: 675.
- Pham, M., Muller, J.F., Brasseur, G., Granier, C., Megie, G., (1995). A three-dimensional study of the tropospheric sulfur cycle, J. Geophys. Res., 100, 26061-26092, 1995.

- Platt, U. (1979) "Simultaneous measurement of atmospheric CH₂O, O₃, and NO₂ by differential optical absorption" Journal of Geophysical Research-Oceans and Atmospheres 84(NC10): 6329.
- Platt, U. (1999) "Modern Methods of the measurement of atmospheric trace gases" Invited Lecture. Physical Chemistry Chemical Physics 1: 5409.
- Platt, U., Perner, D. (1980) "Direct measurements of atmospheric CH₂O, HNO₂, O₃, NO₂, and SO₂ by differential optical-absorption in the near UV" Journal of Geophysical Research-Oceans and Atmospheres 85(NC12): 7453.
- Qian, Y. et al. (2006) "More frequent cloud free sky and less surface solar radiation in China from 1955 to 2000" Geophysical Research Letters (33)
- Roelofs, G.-J., J. Lelieveld, and L. Ganzeveld (1998), Simulation of global sulfate distribution and the influence on effective cloud drop radii with a coupled photochemistry-sulfur cycle model, Tellus, Ser. B, 50, 224– 242.
- Streets, D. G., T. C. Bond, et al. (2003). "An inventory of gaseous and primary aerosol emissions in Asia in the year 2000." Journal of Geophysical Research-Atmospheres **108**(D21).
- Streets, D. G. and S. T. Waldhoff (2000). "Present and future emissions of air pollutants in China: SO₂, NO_x, and CO." Atmospheric Environment **34**(3): 363-374.
- Stutz, J., Platt, U. (1996) "Numerical analysis and estimation of the statistical error of differential optical absorption spectroscopy measurements with least-squares methods" Applied Optics 35(50): 6041.
- Taubman, B. F., L. T. Marufu, C. A. Piety, B. G. Doddridge, J. W. Stehr, and R. R. Dickerson (2004). "Airborne characterization of the chemical, optical, and meteorological properties, and origins of a combined ozone-haze episode over the Eastern United States." J. Atmos. Science **61**: 1781-1793.
- Xu, F., et al. (2007) "Temperature-corrected spectroscopic evaluation method for gas concentration monitoring" Applied Physics B-Lasers and Optics 86(2): 361.
- Yang, K., Personal communication , 22 May 2007